Assessing the influence of NO$_x$ concentrations and relative humidity on secondary organic aerosol yields from α-pinene photo-oxidation through smog chamber experiments and modelling calculations

5 Lisa Stirnweis[1,$], Claudia Marcolli[2,3], Josef Dommen[1], Peter Barmet[1,+], Carla Frege[1], Stephen M. Platt[1,§], Emily A. Bruns[1], Manuel Krapf[1], Jay G. Slowik[1], Robert Wolf[1], Andre S. H. Prévôt[1], Urs Baltensperger[1*] and Imad El-Haddad[1*]

[1]Laboratory of Atmospheric Chemistry, Paul Scherrer Institute, 5232 Villigen, Switzerland

[2]Institute for Atmospheric and Climate Science, ETH Zurich, 8092 Zurich, Switzerland

10 [3]Marcolli Chemistry and Physics Consulting GmbH, Zurich, Switzerland

$Now at: Federal Office for Radiation Protection, Dept. Radiation Protection and Environment, 85764 Oberschleissheim, Germany

+Now at: Department Construction, Traffic and Environment, Canton of Aargau, 5001 Aarau, Switzerland

§Now at: Department of Atmosphere and Climate, Norwegian Institute for Air Research, 2007 Kjeller, Norway

15 *_Correspondence to_: Imad El-Haddad (imad.el-haddad@psi.ch); Urs Baltensperger (urs.baltensperger@psi.ch)

Abstract. Secondary organic aerosol (SOA) yields from the photooxidation of α-pinene were investigated in smog chamber (SC) experiments at low (23-29 %) and high (60-69 %) relative humidity (RH), various NO$_x$/VOC ratios (0.04-3.8) and with different aerosol seed chemical compositions (acidic to neutralized sulfate-containing or hydrophobic organic). A combination of a scanning mobility particle sizer and an Aerodyne high resolution time-of-flight aerosol mass spectrometer was used to determine SOA mass concentration and chemical composition. We used a Monte-Carlo approach to parameterize smog chamber SOA yields as a function of the condensed phase absorptive mass, which includes the sum of OA and the corresponding bound liquid water content. High RH increased SOA yields by up to six times (1.5-6.4) compared to low RH. The yields at low NO$_x$/VOC ratios were in general higher compared to yields at high NO$_x$/VOC ratios. This NO$_x$ dependence follows the same trend as seen in previous studies for α-pinene SOA.

A novel approach of data evaluation using volatility distributions derived from experimental data served as basis for thermodynamic phase partitioning calculations of model mixtures in this study. These calculations predict liquid-liquid phase separation into organic-rich and electrolyte phases. At low NO$_x$ conditions, equilibrium partitioning between the gas and liquid phases can explain most of the increase in SOA yields observed at high RH, when in addition to the α-pinene photo-oxidation products described in the literature, fragmentation products are added to the model mixtures. This increase is driven by both the increase in the absorptive mass and the solution non-ideality described by the compounds' activity coefficients. In contrast, at high NO$_x$, equilibrium

partitioning alone could not explain the strong increase in the yields with RH. This suggests that other processes, e.g. reactive uptake of semi-volatile species into the liquid phase, may occur and be enhanced at higher RH, especially for compounds formed under high NO_x conditions, e.g. carbonyls.

1   Introduction

Organic aerosol (OA) accounts for 20 to 90 % of the submicron ambient aerosol (Jimenez et al., 2009 and references therein), a great part of which is secondary organic aerosol (SOA) formed via the condensation of oxidation products of gas-phase precursors. Several direct (e.g. radiocarbon dating) and indirect observations underline the key role of biogenic volatile organic compounds (VOC) for SOA formation (El Haddad et al., 2013 and references therein). Current state-of-the-art models are unable to predict the burden of biogenic SOA, especially in urban atmospheres (Hoyle et al., 2011), highlighting a fundamental deficit in our knowledge of the chemical pathways by which SOA accumulates and evolves in the atmosphere.

The ensemble of gaseous and particulate phase species involved in SOA formation is immensely complex. The compounds relevant for SOA formation are often a minor fraction, resulting in yields (SOA formed to precursor reacted) of only a few percent. Their chemical composition and volatility distribution strongly depend on the oxidation conditions, most notably on the fate of organic peroxy radicals (RO_2), which either react with nitrogen oxides (NO_x) or other peroxy radicals (RO_2 and HO_2). The influence of NO_x on the oxidation mechanisms and SOA formation is commonly described by the NO_x/VOC ratio and has been under close scrutiny lately. For most light precursors, such as isoprene and monoterpenes (including α-pinene), SOA yields appear to be strongly influenced by the NO_x/VOC ratio, with a general enhancement observed under low NO_x conditions (Ng et al., 2007; Presto et al., 2005).

Species involved in SOA formation are subject to ongoing chemical degradation, which may lead to compounds of either lower (when functionalization dominates) or higher volatility (when fragmentation dominates). As a consequence, SOA yields and degrees of oxygenation (described by the atomic oxygen to carbon ratio O:C) may depend on the extent to which these species were exposed to oxidants (Kroll and Seinfeld, 2008; Donahue et al., 2012a).

SOA yields are generally described by the absorptive equilibrium partitioning of condensable species to a well-mixed liquid phase (Odum et al., 1996), which depends upon the chemical species' saturation vapor pressures (classically two model products are considered) and their liquid-phase activities (modified Raoult's law). Donahue and co-workers proposed the use of a "volatility basis set" (VBS) for a better representation of the wide range of OA in the atmosphere and the ongoing oxidation of semi-volatile organics (Donahue et al., 2011; 2012b and references therein). However, several difficulties remain in estimating or measuring the saturation vapor pressures (e.g. Huisman et al., 2013; Bilde et al., 2015), activity coefficients and the mean molecular weight of the condensing species (e.g. Clegg et al., 2008a, b).

Difficulties increase when considering the role of relative humidity (RH) and of electrolyte particles on organic partitioning (Zuend and Seinfeld, 2013 and references therein). From a thermodynamic point of view, water interacts with SOA components by altering the water content of aerosol particles (also at subsaturated conditions) and hence the equilibrium concentration of water-soluble organic compounds. According to the

equilibrium equation of Pankow (1994), an increase in the condensed fraction of the organics can be achieved by 1) increasing the absorptive particulate mass, 2) decreasing the average molecular weight of condensed species or 3) decreasing the activity coefficients of organic species (Pankow, 1994). Therefore, it is expected that an increase in particulate water content would in principle enhance SOA yields of water-miscible species. Model calculations predict a pronounced effect, especially at low organic mass loadings (Pankow, 2010). However, literature reports based on experimental results seem contradictory: RH dependent yields have been reported for the ozonolysis of limonene, α-pinene and Δ^3-carene (Jonsson et al., 2006), while Prisle et al. (2010) found a negligible impact of RH on SOA yields from α-pinene ozonolysis. A substantial effect of RH on SOA yields was observed only for studies at precursor concentrations <1000 ppbv and with large variation in RH (0.01 % & 31 % RH (Bonn et al., 2002); < 2–58 % RH (Cocker et al., 2001); < 2–85 % RH (Jonsson et al., 2006).

The impact of RH on the partitioning of organic species may be severely suppressed by considerable deviations from ideal mixing between the condensing organic species and the prevailing condensed phase. A growing number of studies show that organic compounds are salted out in internally mixed organic/ inorganic/ water aerosol particles and two stable liquid phases may develop: an aqueous electrolyte solution and an organic solution (Marcolli and Krieger, 2006; You et al., 2014). The miscibility of an organic compound in aqueous droplets containing electrolytes depends on numerous factors including temperature, relative humidity, organic compound polarity, relative contribution of the compound to the bulk particulate matter and the chemical nature of the electrolytes (You et al., 2013; Zuend and Seinfeld, 2013). For example, phase separation was observed to always occur for organic compounds with an O:C < 0.5 and at low relative humidity (You et al., 2013), and is especially pronounced in the case of ammonium sulfate (compared to ammonium hydrogen sulfate and nitrate). While neglecting phase separation of organic compounds and the effect of RH thereon bears the potential for invalid yield predictions (e.g. if the condensed phase is considered to comprise a mixed electrolyte and organic solution), the way the complex organic matrix interacts with water and the inorganic species remains virtually unknown.

Another complication that might influence the interpretation of chamber experiments conducted at different RH is the enhancement of SOA yields by the potential reactive uptake of organic products into the particle phase (Kroll and Seinfeld, 2008; Kleindienst et al., 2006; Jang et al., 2002; Iinuma et al., 2007). The mechanisms by which such reactions occur are not fully identified, but may involve an ester or an aldol formation, which are expected to be favourable in the absence of water and are possibly catalytic under acidic conditions. Assessing the relative importance of particle phase processing at different particle water contents would require decoupling SOA thermodynamics and additional reactivity.

In this study, we examine the impact of particle water content on the chemical composition and yields of α-pinene SOA formed under low and high NO_x. This is performed by varying NO_x/α-pinene ratios, aerosol seed composition (hygroscopicity, acidity) and relative humidity. Results are parameterized within a thermodynamic framework to investigate whether changes in SOA non-ideal mixing properties with particle water content may explain the variation in SOA yields with RH. SOA yields reported here may aid the parameterization of the NO_x and particulate water dependence of α-pinene SOA production for further use in atmospheric models.

2 Methods

2.1 Experimental setup and instrumentation

20 experiments, listed in Table 1, were carried out in the smog chamber (SC) of the Paul Scherrer Institute (PSI): a Teflon bag of 27 m³ suspended in a temperature-controlled housing (Paulsen et al., 2005). Photochemistry was initiated by four xenon arc lamps (4 kW rated power, $1.55 \cdot 10^5$ lumens each, XBO 4000 W/HS, OSRAM), facing parallel to the SC bag, and emitting a light spectrum similar to the solar spectrum, and 80 black lights (Philips, Cleo performance 100 W) to accelerate the aging process, located underneath the SC bag, with emission between 300–400 nm wavelength (light characterisation in Platt et al. (2013)). A reflecting aluminum foil surrounds the SC bag to maintain light intensity and light diffusion.

Various parameters were monitored in the SC. The temperature (T) and RH measurement was optimized by passing SC air through a radiation shielded sensor. One of two different high resolution time-of-flight aerosol mass spectrometers (HR-ToF-AMS, Aerodyne Research, Inc., Billerica, MA, USA) was operated during three different campaigns to measure online size-resolved chemical composition (organics, ammonium, nitrate, sulfate, chloride) of non-refractory particles (DeCarlo et al., 2006). The HR-ToF-AMS were equipped with two different $PM_{2.5}$ lenses (Williams et al., 2013) to sample particles up to large diameters above 1 µm. The sampled aerosol was dried (~10 % RH) before measurement. A supporting flow of ~1.5 L min^{-1} was maintained parallel to the HR-ToF-AMS to minimize diffusive losses in the sampling lines.

The HR-ToF-AMS data were processed and analysed using the analysis software SQUIRREL (SeQUential Igor data RetRiEvaL) v.1.52L and PIKA (Peak Integration by Key Analysis) v.1.11L for IGOR Pro software package (Wavemetrics, Inc., Portland, OR, USA). From the HR analysis of the mass spectra, the O:C ratios of the bulk OA were determined based on the parameterization proposed by Aiken et al. (2008). We note that while the assessment of the uncertainties related to the O:C measurements by the HR-ToF-AMS is not straightforward, a distinction should be made between measurement precision and accuracy. We do not expect the accuracy of the O:C ratios determined by the HR-ToF-AMS to be less than ~20 % (Aiken et al., 2008; Pieber et al., 2016; Canagaratna et al., 2015; Bozzetti et al., 2017). For example, the use of a more recent parameterization (Canagaratna et al., 2015) would yield higher O:C values (by 18 %) and the O:C ratios reported here may be regarded as lowest estimates. By contrast, relative changes in the O:C ratios are expected to be detected more precisely by the instrument (~1-2 %). The influence of potential biases and uncertainties in the determination of the O:C ratios on our results will be discussed in the text.

Two scanning mobility particle sizers (SMPS) were additionally deployed for the measurement of the aerosol size distributions. The first SMPS (a custom built differential mobility analyzer, DMA: extended length $L_{eff} =$ 0.93 cm, $d_{m\,max}$=1000 nm, recirculating sheath flow, and a condensation particle counter, CPC 3022 (TSI)) was connected to the HR-ToF-AMS sampling line to analyze the dried particles. A second SMPS (SMPS$_{wet}$, a TSI DMA classifier 3081 with recirculating sheath flow and a TSI CPC 3022A) and a CPC (TSI: CPC 3025A) measured the wet particle number size distribution and total number concentration ($d > 3$ nm), respectively.

Gas-phase compounds with a higher proton affinity than water (166.5 kcal mol^{-1}) were measured with a quadrupole proton transfer reaction mass spectrometer (PTR-MS, Ionicon). The PTR-MS was calibrated before each experiment for α-pinene, detected at *m/z* 137 and *m/z* 81; the accuracy of these measurements was estimated to be ~5 %, based on the purity indicated on the calibration gas cylinder.

A modified NO_x instrument including a photolytic NO_2-to-NO converter (Thermo Environmental Instruments 42C trace level NO_x analyzer equipped with a blue light converter) and two ozone monitors (Monitor Labs 8810 ozone analyzer, Environics S300 ozone analyzer) monitored NO_x and O_3 in the chamber.

2.2 Chamber operation and aerosol seeding

5 SOA formation and growth from α-pinene was induced by the following SC operation sequence: (1) humidification of the chamber, (2) addition of seed aerosol, (3) introduction of VOCs, (4) addition of nitrous acid (HONO) as an OH precursor, (5) addition of nitrogen oxides (equal amounts of $NO + NO_2$) if applicable, (6) an equilibration period (30–45 min), (7) switching on of xenon and black lights to generate OH radicals, and (8) a reaction time of 5 to 20 h (corresponding to $0–2 \times 10^8$ cm^{-3} h OH exposure, see Sect. 2.4). Experimental
10 conditions for each individual experiment are summarized in Table 1. Prior to each experiment, cleaning of the SC was performed by the injection of several ppmv of ozone (5 h) and the simultaneous irradiation with black lights (10 h) at a temperature of 20 °C. This was followed by a pure air flushing period at high relative humidity (~60 %) at a temperature of approximately 30 °C for at least 20 h. Three blank experiments (seed aerosol, lights switched on, high RH, but without adding α-pinene) were carried out to make sure that the organic aerosol
15 formed during the experiments is not significantly influenced by background contamination in the SC. The organic mass concentration formed was substantially lower (< 0.1 up to 2.8 µg m^{-3}) than during comparable experiments (similar NO_x and RH).

In the chamber, the temperature varied between 21 °C and 26 °C. Due to heat from the xenon and black lights, the temperature increased, stabilizing only ~1 h after experiment start. The increase in temperature of 1–4 °C led
20 to an absolute decrease in RH of ~2-20 %, thus the RH range in Table 1, 23–67 %, is given for the stable temperature period. α-Pinene (98 %, Aldrich) and an OH reactivity tracer (9-times deuterated butanol, 98 %, D9, Cambridge Isotope Laboratories), hereafter referred to as butanol-d9 (1 µL injected ≈ 10 ppbv in the SC), were sequentially injected into an evaporation glass bulb heated to 80 °C. The two VOCs were transferred into the bag by a dilution and flush flow (each 15 L min^{-1}, maintained for 15 min) from an air purifier (737-250 series,
25 AADCO Instruments, Inc., USA), further referred to as "pure air". Initial α-pinene concentrations were 16.1– 31.7 ppbv.

HONO was used as a source of both NO and OH, produced by continuous mixing in a reaction vessel of the reagents sodium nitrite (NaNO$_2$, 1 mmol L^{-1} in milliQ-H$_2$O) and three different concentrations of sulfuric acid solutions (H$_2$SO$_4$, 1 mmol L^{-1} (expts. 1-6), 10 mmol L^{-1} (expts. 7, 8, 11, 13) and 100 mmol L^{-1} (expts. 9, 10, 12,
30 14) in milliQ-H$_2$O) (Taira and Kanda, 1990). HONO was carried by 2.5 ± 0.2 L min^{-1} pure air flow into the SC. 2 ppbv (± 10 %) of HONO were injected before lights on to initiate photochemistry and the injection was continued throughout all experiments. A chemiluminescence-based NO_x instrument (Monitor Labs 9841A NO_x analyzer) was attached to the HONO source to monitor the injected concentration throughout the experiment. In addition, equal concentrations of NO (99.8 %; 1005 ppmv ± 2 %) and NO$_2$ (purity: 98 %; 1005 ppmv ± 3 %),
35 resulting in 19.6–75.1 ppbv initial NO_x, were added during experiments with NO_x/α-pinene > 1. Within the results section, the two terms "low NO_x" and "high NO_x" refer to the following conditions:

- Low NO_x = NO_x/α-pinene < 0.1, with continuous HONO injection, indicated by an asterisk in Table 1 and figures.

- High NO_x = NO_x/α-pinene > 1: Initial injection of $NO + NO_2$ with continuous HONO injection.

In Table 1, we report for high NO_x conditions the initial NO_x concentration, (which decays with time) and for low NO_x conditions the mean NO_x concentration. We note that the NO levels are the main driver for determining whether RO_2-NO or RO_2-RO_2 reactions would prevail. Based on our calculations (not shown here, see Platt et al., 2014), RO_2 radicals would predominantly react with NO, when the concentration of the latter is higher than

5 only 1 ppb. These conditions can be considered as high NO_x. During high NO_x experiments and throughout the period when the majority of α-pinene was consumed, the NO concentration remained higher than 5ppb, indicating that α-pinene oxidation proceeded under high NO_x. During low NO_x experiments, the average NO_x concentration was around 1-2 ppb, predominated by NO_2, while the NO concentrations were below detection limits (<0.1ppb). Under these conditions RO_2-RO_2 reactions may prevail.

10 During 14 experiments (no. 1–14) and three blank experiments, an ammonium hydrogen sulfate (NH_4HSO_4, Aldrich) solution in ultrapure Milli-Q water (1 g L^{-1}) was nebulized (0.6 L min^{-1}) and introduced into the SC with a pure air dilution flow of 10 L min^{-1} to act as seed particles. To keep the seed aerosol in a liquid state, no drier was used behind the nebulizer. We determined the acidity of the seed particles, here described by the ratio NH_4/SO_4, by the comparison between the HR-ToF-AMS measurements of the seed particles and nebulized

15 $(NH_4)_2SO_4$ and NH_4HSO_4 solutions. An NH_4/SO_4 ratio between 1 and 2 indicates a rather neutral seed composition, representing a mixture of NH_4HSO_4, $(NH_4)_3(SO_4)_2$ (letovicite) and $(NH_4)_2SO_4$. For simplicity, we replaced $(NH_4)_3(SO_4)_2$ by an equal mix of NH_4HSO_4 and $(NH_4)_2SO_4$ for the assumption of density and growth factors. By contrast, an $NH_4/SO_4 \leq 1$ indicates an acidic seed, consisting of NH_4HSO_4 and H_2SO_4.

During experiments 7–14, the nebulized NH_4HSO_4 solution was partly neutralized to $(NH_4)_2SO_4$, presumably by

20 background NH_3 (Fig. S1, Supplement). During experiments 1–6 the seed was composed of an aqueous mixture of NH_4HSO_4 and H_2SO_4, due to the in–situ production of gas-phase H_2SO_4 via the HONO injection system, suppressing the seed neutralization by NH_3 (even though particulate H_2SO_4 was minimised by a teflon filter applied between the HONO source and the SC).

Additionally, three α-pinene experiments (no. 15–17) and one blank experiment were conducted using an inert

25 hydrophobic fluorinated hydrocarbon seed (further referred to as CF-seed; $CF_3CF_2CF_2O$-[CF(CF_3)CF_2-O-$]_nCF_2CF_3$; Krytox® 1525). The CF-seed was generated via the evaporation of the pure compound at a temperature of 125–145 °C and subsequent homogeneous nucleation in a pure air flow of 2.4 ± 0.1 L min^{-1}. The CF-seed concentration was 6.7–10 µg m^{-3} when lights were switched on, and decayed very rapidly to values below detection limit of the HR-ToF-AMS (0.1 µg m^{-3}) during the course of the experiment. The CF-seed mass

30 spectrum in the HR-ToF-AMS is clearly distinct from that of α-pinene SOA, with main contributions at *m/z* 69 (CF_3), *m/z* 169 (C_3F_7) and *m/z* 119 (C_2F_5) (Fig. S2 and Table S1, Supplement).

Table 1 lists the expected physical state and seed composition of each experiment dependent on RH (AHS = ammonium hydrogen sulfate (NH_4HSO_4); AS = ammonium sulfate (($NH_4)_2SO_4$); SA = sulfuric acid (H_2SO_4); CF = fluorinated carbon. Submicrometer AS particles and letovicite particles (($NH_4)_3H(SO_4)_2$) are expected to

35 effloresce at about 35 % RH while more acidic particles should remain liquid between 20 and 30 % RH (Martin, 2000; Ciobanu et al., 2010).

2.3   Estimation of the hygroscopic growth factors and liquid water content

The absolute liquid water content (LWC) of the aerosol particles was derived for the bulk aerosol mass and the size resolved mass distribution, based on literature growth factors, the measured RH and chemical composition.

The growth factor GF (RH) of a particle is defined as the ratio of the wet diameter at a given RH to the dry diameter: $GF(RH) = d(RH)/d_{dry}$. Inorganic GFs were taken from the Aerosol Diameter Dependent Equilibrium Model (ADDEM, Topping et al., 2005) for diameters of 360 nm. Organic GFs were derived using the relationship between the hygroscopicity parameter κ and the degree of oxygenation [$\kappa = 0.29\times(O:C)$] from Chang et al. (2010), well representing the hygroscopicity of α-pinene SOA measured by Massoli et al. (2010). The measured degree of oxygenation at an OH exposure of $(2.0 \pm 0.5) \times 10^7$ cm^{-3} h was used to derive κ, which in turn was converted to GF, assuming a negligible curvature (Kelvin) effect (Kreidenweis et al., 2005):

$$GF(RH) = \left(1 + \kappa \frac{\frac{RH}{100\%}}{1 - \frac{RH}{100\%}} \right)^{\frac{1}{3}} \tag{1}$$

The mixed GFs for aerosol containing inorganic and organic species were determined using as a first approximation the Zdanovskii-Stokes-Robinson (ZSR) volume mixing rule (Stokes and Robinson, 1966):

$$GF_{mixed}(RH) = \left(\sum_i \varepsilon_i \times \left(GF_i(RH) \right)^3 \right)^{\frac{1}{3}} \tag{2}$$

where ε_i and $GF_i(RH)$ denote the volume fraction and GF (RH) of species i, respectively. The H$_2$O volume (V_{H_2O}) was calculated using the definition of GF (RH) and the dry volume (V_{dry}):

$$V_{H_2O} = V_{dry} \times (GF(RH)^3 - 1) \tag{3}$$

V_{H_2O} multiplied by the density of water (1 g cm^{-3}) results in the LWC.

The dry (S_{dry}) and wet (S_{wet}) surfaces from HR-ToF-AMS size resolved data were calculated with Eq. (4) and Eq. (5), respectively:

$$S_{dry} = 6 \times (V_{dry})/d_{dry} \tag{4}$$

$$S_{wet} = 6 \times (V_{dry} + V_{H_2O})/(d(RH)) \tag{5}$$

The LWC and surface distributions were calculated using size resolved pToF (particle time-of-flight) data of the HR-ToF-AMS. Due to the low pToF signal of NH$_4$, the NH$_4$ surface distributions were estimated based on SO$_4$ pToF measurements.

2.4 Determination of OH exposure and extent of α-pinene ozonolysis

The gas-phase composition, the OH concentration and the photochemical age of a chemical reaction system may considerably differ between experiments of the same duration. Furthermore, variation of the OH concentration within a single experiment means that the photochemical age is not necessarily directly proportional to the light exposure time. Consequently, we discuss reaction time in terms of OH exposure (molecules cm^{-3} h), defined as the OH concentration integrated over time. OH exposures were derived based on the decay of the OH tracer butanol-d9, detected by the PTR-MS as M+H$^+$-H$_2$O at m/z 66), following the methodology introduced by Barmet et al. (2012). The OH exposure was determined by the integration of the following expression:

$$\text{OHexposure} = -\int_{t_1=0}^{t} \left(\frac{1}{k_{OH,butanol-d9}} \cdot \left(\frac{\Delta \ln(butanol-d9)}{\Delta t} + \frac{f_{dil}}{V} \right) \right) dt \tag{6}$$

where butanol-d9 and $k_{OH, butanol-d9}$ (= 3.4×10^{-12} cm^3 molecules^{-1} s^{-1}) are the butanol-d9 concentration and its reaction rate constant against OH, respectively, t is the time after lights on, V the chamber volume (we assume as

a first approximation a constant chamber volume of 27 m³), and f_{dil} the dilution flow due to HONO input (Sect. 2.2).

The percentage of α-pinene reacted with OH and O₃ was derived based on Eq. (7):

$$-\frac{d\,(\alpha-pin)}{dt} = k_{O_3,\alpha-pin}\,[O_3] \times [\alpha - pin] + k_{OH,\alpha-pin}\,[OH] \times [\alpha - pin] + \frac{f_{dil}}{V} \tag{7}$$

5   where [α-pin], [O₃] and [OH] denote the concentrations of α-pinene (measured by the PTR-MS at *m/z* 137 and 81), O₃ and OH, respectively, and $k_{OH,\,\alpha-pin}$ (= 5.3×10^{-11} cm³ molecules⁻¹ s⁻¹) and $k_{O3,\,\alpha-pin}$ (= 8.9×10^{-17} cm³ molecules⁻¹ s⁻¹) the reaction rate constants of α-pinene with OH and O₃, respectively. The percentage of α-pinene reacted with OH is presented in Table 1 and discussed in Section 3.4.

2.5   Determination of suspended and wall-loss-corrected organic masses and yields

10   ***Suspended OA mass.*** The suspended organic mass concentration C_{OA}^{sus} was derived by utilizing the chemical composition measurements from the HR-ToF-AMS scaled to the total volume measured by the SMPS (Fig. S3 and Fig. S4, Supplement), using compound-specific densities (ρ_{org} = 1.4 g cm⁻³, $\rho_{NH4HSO4}$ = 1.79 g cm⁻³, $\rho_{(NH4)2SO4}$ = 1.77 g cm⁻³, ρ_{H2SO4} = 1.83 g cm⁻³).

For some experiments (9, 10, 12 and 14-17), the organic mass concentrations determined by the HR-ToF-AMS
15   were corrected for a sub-unity transmission efficiency at the lower edge cut-off of one of the two PM₂.₅ lenses employed (Fig. S3 and Fig. S4, Supplement). Additionally, for organic mass calculation, we assumed that the measured NO₃ signals are entirely related to organonitrates (RONO₂), rather than NH₄NO₃. This assumption mainly stems from (1) the observation of the NO₃ signal in the same particle size region as OA rather than SO₄²⁻ (see size-resolved pToF data, Sect. 3.3), while inorganic nitrate would be expected to mix within an electrolyte
20   rich aerosol and (2) the presence of NO₃ under acidic conditions, which are thermodynamically unfavorable for the partitioning of nitric acid. This is also supported by the higher NO⁺/NO₂⁺ ratios measured in the SC compared to ratios recorded during NH₄NO₃ nebulization (on average 1–2.8 times higher, Supplement Fig. S5), typically expected from organonitrates (Farmer et al., 2010). We cannot exclude that a part of the NO₃ signal originates from NH₄NO₃. However, even attributing all detected nitrate to NH₄NO₃ would increase the
25   calculated LWC by 1–13 % and decrease the calculated OA mass by 2–7 % only, which would not influence our conclusions. Finally, for yield calculations we assume the accuracy of the aerosol phase measurements to be 30% (Canagaratna et al., 2007).

Wall-loss-corrected OA mass. To obtain the total C_{OA} concentration corrected for losses of particles and vapors to the chamber walls, we use Eq. (8), introduced by Hildebrandt et al. (2011), based on the mass balances of the
30   suspended organic aerosol mass, C_{OA}^{sus}, and the mass of the organic aerosols on the walls, C_{OA}^{walls} (summed up to derive C_{OA}):

$$\frac{d}{dt}\left[C_{OA}^{walls}(t)\right] = k_{OA}^{w}(t)C_{OA}^{sus}(t) + \omega(t)\cdot\left(k_{OA}^{w}(t)C_{OA}^{sus}(t) + \frac{d}{dt}\left[C_{OA}^{sus}(t)\right]\right)\cdot\frac{C_{OA}^{walls}(t)}{C_{OA}^{sus}(t)} \tag{8}$$

Here, k_{OA}^{w} represents the loss rate constant of organic particles to the walls, derived by fitting the suspended organic mass concentration 5–8 h after lights were switched on in the SC, when SOA production is expected to
35   be negligible (α-Pinene concentration < 1 ppbv, Fig. S6 and Table S2, Supplement). We determine an average loss rate of 0.13 µg m⁻³ h⁻¹, corresponding to a particle half-life of 5.3 h. The average k_{OA}^{w} was used in the case of insufficient statistics to perform accurate fitting. In Eq. (8), ω, ranging between 0 and 1, is a dimensionless

proportionality coefficient between the mass of organic vapors that partition onto the wall-deposited particles and the mass of organic vapors that partition onto the suspended particles. Here, we neglect the condensation of organic vapors onto the wall-deposited particles, i.e. $\omega = 0$, consistent with previous studies of α-pinene SOA production (Hildebrandt et al., 2011 and references therein). This assumption gives a lowest estimate of SOA yields, but does not influence the comparison between the experiments. Considering the second limiting case $\omega = 1$, i.e. an equal partitioning of organic vapors between the wall-deposited and suspended particles, would increase the determined SOA yields (by up to 40 %, and by 20 % on average).

Eq. (8) does not take into consideration the loss of SOA-forming vapours onto the clean Teflon walls, which may suppress SOA yields from laboratory chambers under certain conditions. These processes may be related to the vapours' reactive uptake onto walls (Loza et al., 2010; Nguyen et al., 2016) or to their absorptive uptake (Zhang et al., 2014; Nah et al., 2016). The reactive uptake of organic vapours onto chamber walls is only significant at high RH. Loss rates for important reactive gases, including glyoxal, epoxides and peroxides have been documented at different RH (Loza et al., 2010; Nguyen et al., 2016). While these processes may also influence reactive SOA-forming compounds under our conditions, they occur at time-scales of hours (Nguyen et al., 2016), much longer compared to the time scales of the absorptive uptake, e.g. based on recent direct measurements of vapour losses onto Teflon walls (~10 min (Krechmer et al., 2016)).

The absorption of organic compounds onto the chamber walls obeys Henry's law and depends on the compounds' accommodation coefficients and their activity at the wall/gas interface (see for example Zhang et al., 2015). The dependence of the compounds' absorption on RH (due to a change in accommodation coefficients or in the activity of the wall absorbed compounds) has not yet been reported to the best of our knowledge and indeed merits further investigations that are beyond the scope of the current study. Nevertheless, we believe that vapour absorption onto the walls is unlikely to be significantly affected by RH, due to the hydrophobic nature of Teflon and its minor interaction with water under subsaturation conditions (RH < 80 %). In our case, we have maintained chamber conditions during our experiments such that vapour wall losses and their inter-experimental differences can be minimized as much as possible. This is done by (1) maintaining a relatively constant wall-to-seed surface ratio for all experiments to avoid systematic biases between experiments and (2) increasing SOA production rates, which rapidly provide a significant particle condensational sink into which condensable gases can partition. We also note that vapour wall losses were found to be minor for the α-pinene SOA system where SOA formation is dominated by quasi-equilibrium growth (Zhang et al., 2014; Nah et al., 2016).

SOA yields determination and parameterization. SOA mass yields, *Y* (dimensionless quantity), are calculated from Eq. (9), as the organic mass concentration formed, C_{OA}, per precursor mass consumed, $\Delta C_{α\text{-}pinene}$:

$$Y = \frac{C_{OA}}{\Delta C_{α-pinene}} \tag{9}$$

For comparison purposes, *Y* values are reported in Figure 2 and Table 1 and discussed in Sect. 3 at an OH exposure of $(2.0 \pm 0.5) \times 10^7 \, \text{cm}^{-3}\,\text{h}$, reached during all experiments. The parameterization of smog chamber SOA yields measured is based on the absorptive partitioning theory of Pankow (Eq. (10)), which expresses the production of a set of semi-volatile surrogate products (total number *N*) as a function of the mass yield of these products, $α_i$, and their partitioning coefficients, ξ_i (a dimensionless quantity reflecting the condensed-phase mass fraction of these products). The critical parameters driving the partitioning of these products are their effective saturation concentration, C_i^*, and the total concentration of the absorptive organic phase, C_{OA}. As discussed

below, we consider the absorptive organic mass as the sum of the total OA concentration and the liquid water in this phase (Sect. 3.3).

$$Y = \sum_i^N \alpha_i \xi_i = \sum_i^N \alpha_i \left(1 + \frac{c_i^*}{c_{OA}}\right)^{-1} \tag{10}$$

In Eq. (10), C_i^* (in µg m^{-3}) is a semi-empirical property (inverse of the Pankow-type partitioning coefficient, $K_{P,i}$) reflecting the saturation vapor pressure of the pure constituents $\left(p_{L,i}^o\right)$ and the way they interact with the organic mixture (effectively including liquid phase activity coefficients, γ_i), as expressed in Eq. (11):

$$C_i^* = \frac{10^6 M_i \gamma_i P_{L,i}^o}{760RT} \tag{11}$$

Here, M_i denotes the compound molecular weight, R the ideal gas constant and T the temperature. Smog chamber yields from single experiments are fitted as a function of C_{OA} using the volatility basis set (VBS) (Donahue et al., 2006), which separates semi-volatile organics into logarithmically spaced bins of effective saturation concentrations C_i^*. Figure 5 shows the resulting parameterizations (lines) in comparison to the measured data (symbols) for each experiment.

To determine the yields per volatility bin (α_i), wall-loss-corrected SOA yields, Y as a function of wall-loss-corrected absorptive mass concentration C_{OA} (data presented in Figure 5) were used. We assumed a total number of 5 bins: $N = 5$ with $C_i^* = 0.01, 0.1, 1, 10$ and 100 µg m^{-3}. To solve Eq. (10) for the parameters α_i, we introduced a novel approach using a Monte Carlo simulation. This approach provides best estimates of α_i values (data shown in Figure 6 and Fig. S7 in the Supplement), together with a measure for the uncertainties related to the determination of the volatility distributions from SC experiments. The calculation proceeded as follows:

1/ From the calculated yields (Y), lower (Y_1) and upper (Y_2) yield curves were determined based on the estimated measurement accuracy of C_{OA} and α-pinene mass. A possible yield domain was inscribed against C_{OA} by plotting Y_1 and Y_2 vs. their corresponding lower and upper C_{OA}, respectively. The parameterized yield curves are shown in Figure 5.

2/ A range of possible inputs was defined for each of the parameters α_i. This range is restricted within the following interval [0; 2*(Y_i - Y_{i-1})]. This step was only necessary for computational reasons.

3/ α_i-parameters were randomly generated over the defined intervals.

4/ Deterministic computations of Y vs. C_{OA} were performed using Eq. (10) and the generated α_i inputs.

5/ Volatility distributions that fell within the domain defined in step (1) were retained, aggregated and presented as probability distribution functions for each of the five effective saturation concentrations C_i^* (probability density function, PDF, Figure 6 and Fig. S7 in the Supplement).

2.6   Thermodynamic modelling

General principles. Using thermodynamic modelling, we seek to understand whether observed changes in SOA bulk properties (yields and O:C ratios) with RH can be explained by a change in the particles' thermodynamic properties. Gas-liquid and liquid-liquid phase partitioning calculations are performed following the methods developed in Zuend et al. (2008; 2010; 2012) and Zuend and Seinfeld (2013), using the thermodynamic group-contribution model, AIOMFAC (Aerosol Inorganic-Organic Mixtures Functional groups Activity Coefficients)

to calculate activity coefficients. This approach enables predicting the phase partitioning of known organic compounds knowing their abundances in a given known mixture of organic species and electrolytes at a given RH and temperature.

The modelling requires the use of explicit surrogate compounds. Based on Eq. (10), the partitioning of these compounds is driven by their volatility distributions, which depends on (1) the compounds' effective saturation concentrations and (2) their relative abundances. Compounds' effective saturation concentrations, used as model inputs, were calculated based on Eq. (11) initially assuming ideal mixing ($\gamma=1$) and utilizing vapor pressures estimated using EVAPORATION (Compernolle et al., 2011). The relative abundances of these compounds in the model mixtures are based on the volatility distributions derived from experimental data (section 2.5).

We assumed instantaneous reversible absorptive equilibrium of semi-volatile organic species into ideal and non-ideal liquid phase aerosols. In the case of non-ideal solutions, positive and negative deviations of mole fraction-based activity coefficients from unity indicate the degree of non-ideality in a mixture. The activity coefficients take into account the compounds' affinity towards the solution (interactions with other organic species, electrolytes and water) and hence depend on the solution chemical composition. Therefore, the activity coefficients for the different organic species cannot be set *a priori*, but are calculated iteratively in the model (until convergence of the compounds' abundances in the different phases; see (Zuend et al., 2008; Zuend et al., 2011).

We considered cases with and without interactions between the electrolyte and the organic phases, which enables assessing the solubility of the organic compounds in the inorganic seed aerosols. Seed concentrations in μg m^{-3} were transformed in moles of seed per volume (mol m^{-3}) assuming equal shares of AHS and SA for acidic seeds and equal shares of AHS and AS for neutral seeds. Because interaction parameters of some organic functional groups with HSO_4^- are missing in AIOMFAC, we assumed the interactions of organic compounds with HSO_4^- and with SO_4^{2-} to be similar. For all computations, metastable supersaturated salt solutions were allowed.

Model compounds are only surrogates. The choice of these surrogates should reflect the wide range of volatility and hydrophilicity of SOA species. We have selected as surrogates α-pinene photo-oxidation products reported in literature, identified under different NO_x and aerosol seed conditions, covering the wide range of volatility relevant to SOA. Compound hydrophilicity instead depends heavily on the number of functional groups present in the molecule, which can be largely simulated by the compound O:C ratio (Zuend and Seinfeld, 2012). As increasing the compound O:C ratio also decreases its volatility, we have considered cases with and without fragmentation products with shorter carbon backbone chain, but high O:C ratios, expected to be representative of later generation photolysis and photo-oxidation products (Mutzel et al., 2015; Krapf et al., 2016). This approach would effectively decouple compounds' hydrophilicity and volatility and allow scanning both properties independently. While we recognize that oxidation conditions, e.g. NO_x concentrations, may significantly alter the product distribution, we did not select different sets of products for the different conditions. This is because:

(1) such separation would implicitly suggest that the chemical composition of the few compounds reported at different conditions can be extrapolated to the bulk OA under our conditions;

(2) such separation would significantly limit the number of surrogates at each condition, increasing the sensitivity of the model to the compounds' selection;

(3) the model is less sensitive to compounds' chemical structure than to their elemental composition (see below and Li et al. (2016)), e.g. number of oxygen and carbon, which has been taken into account by including fragmentation products.

The relative abundance of the selected compounds is optimized in the model for each experiment at the prevailing RH such that the modelled and measured SOA yield and O:C ratio match. Then, the RH is modified in the model, and changes in the SOA yields and O:C ratios are compared to the observations. Model calculations were performed at an OH exposure of $(2.0 \pm 0.5) \times 10^7$ cm^{-3} h. In the following we thoroughly describe the different steps involved in the model setting.

Simulated cases. The following simulations were performed:

1/   Case org: non-ideal partitioning including liquid-liquid phase separation, LLPS (activity coefficients calculated with AIOMFAC) of the organic compounds between gas phase and a purely organic aerosol phase neglecting the presence of the seed aerosol and using reported model compounds only;

2/   Case id: ideal partitioning (activity coefficients all set to unity, LLPS cannot occur) between gas phase and organic aerosol phase using reported model compounds only;

3/   Case sd: non-ideal partitioning including the seed aerosol to an internally mixed organic/AS aerosol using reported model compounds only;

4/   Case sdfr: non-ideal partitioning including the seed aerosol to an internally mixed organic/AS aerosol including the formation of fragmented oxidation products (see below);

5/   Case orgfr: non-ideal partitioning including LLPS to a purely organic aerosol phase neglecting the presence of the seed including the formation of fragmented oxidation products.

α_i-parameters determined through the Monte-Carlo simulations assume that the absorptive mass consists of the organic phase (in accordance with assumptions in chemical transport models). This assumption is violated for cases sd and sdfr as compounds may partition into the inorganic phase. Nevertheless, the results obtained for these cases may still be examined in relative terms to inspect the effect of RH on SOA yields in the presence of an inorganic seed and the partitioning of SOA compounds between the inorganic and organic phases.

Model compounds. To simulate SOA partitioning in AIOMFAC, α-pinene photooxidation products reported in the literature (Eddingsaas et al., 2012; Jaoui and Kamens, 2001; Kleindienst et al., 2007; Valorso et al., 2011) were chosen as model compounds for cases org, id and sd, namely ValT4N10 (10th compound in Table 4 from Valorso et al. (2011)), 3-hydroxyglutaric acid, pinic acid, hopinonic acid, norpinic acid, 2-hydroxyterpenylic acid, 10-oxopinonic acid, and 4-oxopinonic acid. These compounds are listed in Table S4 in the Supplement together with their relevant physicochemical properties (MW, O:C ratio, vapor pressures and chemical structures). For cases sdfr and orgfr additional oxidized fragmented products (3-oxoadipic acid, glutaric acid, 5-COOH-3-OH-pentanal, and succinic acid) were included (Table S4, Supplement). While these compounds were not reported to derive from α-pinene oxidation, their structure, including carbon and oxygen numbers are very similar to the most abundant compounds detected by Chhabra et al. (2015) and Mutzel et al. (2015) using chemical ionization mass spectrometry. Volatility distributions could reliably be determined for volatility bins $C^* = 0.1$-100 µg m^{-3}. Nevertheless, also lower volatility products with $C^* = 0.01$ µg m^{-3} are formed. Therefore, this bin was loaded for all phase partitioning calculations with equal fractions of the model compounds

diaterpenylic acid acetate, 3-MBTCA and ValT4N9 with mass yields of 10^{-5} each. This low mass fraction does not influence the organic yield but proved to aid the convergence of the phase partitioning calculation. To achieve mass closure in the model, pinonaldehyde (MW: 168 g mol^{-1}) was assumed to represent the more volatile products, which do not partition to the condensed phase. Because pinonaldehyde resides almost totally in

5   the gas phase, it was not explicitly modelled.

Model compounds C_j^* calculation. Model compounds j were assigned to the volatility bins based on the calculated C_j^* values using Eq. (11) and assuming ideal mixing ($\gamma_j = 1$). Using the actual activity coefficients calculated with AIOMFAC is not possible because they are a result of the phase partitioning calculation. However, because activity coefficients proved to be generally in the range of 0.1 to 10, they did not alter the

10   initial product assignments to the volatility bins which cover one order of magnitude in effective saturation concentration. Therefore, the initial allocation of the compounds to the volatility bins in the VBS remains valid after taking the non-ideality into account. $p_{L,j}^o$ used in the calculations were vapor pressures of pure compounds in liquid or subcooled liquid state, at 298 K estimated using EVAPORATION (estimation of vapor pressure of organics, accounting for temperature, intramolecular, and non-additivity effects, (Compernolle et al., 2011)),

15   without using the empirical correction term for functionalized diacids.

Setting model compounds' relative abundances in the model. From the α_i-parameters generated through the Monte Carlo simulations in Sect. 2.5, 10 sets per experiment were randomly selected for the phase partitioning calculations (provided that these parameters fall within the 10th and the 90th percentiles, to avoid outliers). The 11 chosen experiments exclude experiments 15-17 with hydrophobic seeds, experiment 6 which has no

20   counterpart experiment at high RH and experiments 5 and 14 where the COA concentration range was very limited to accurately derive αi-parameters (Sect. 2.5). The chosen parameters are listed in Table S5 in the Supplement. As several model compounds are assigned to a volatility bin i, the yield of a compound j is expressed as its relative contribution within the volatility bin i, $\chi_{j,i}$, times the relative abundance of the bin α_i. For each experiment and each simulated case the fitted $\chi_{j,i}$ values are listed in Tables S6-S8 in the Supplement.

25   For case org the $\chi_{j,i}$-values were optimized to match the experimental organic yields and the measured O:C at the actual RH of the experiment. RH was then changed in the model and the effects of RH on SOA yields and degree of oxygenation were evaluated. For cases id and sd the same $\chi_{j,i}$ were used as for case org. For cases sdfr and orgfr, more fragmented compounds were added and their $\chi_{j,i}$-values were optimized to achieve agreement between measured and modelled organic mass yields and O:C ratios. Likewise, the effects of RH on SOA yields

30   and on O:C ratios were then evaluated by changing the RH in the model.

The following pairs of corresponding experiments were simulated: experiments 3 and 4 (66 % RH, 29 % RH), experiments 7 and 11 (67 % RH, 26 % RH), experiments 8 and 13 (60 % RH, 25 % RH), and experiments 10 and 12 (50 % RH; 26 % RH). Equilibrium calculations were performed starting from both, low and high RH experiments. For experiments 5 and 14 performed at low RH values, the volatility distribution parameters could not

35   be determined for the most volatile bin (α_5). Therefore, equilibrium partitioning calculations were only performed starting from their corresponding experiments, namely experiment 1 (69 % RH), experiment 2 (67 % RH), and experiment 9 (56 % RH).

3 Experimental results

Figure 1 shows the suspended and wall-loss-corrected organic mass concentrations for all experiments listed in Table 1 as a function of OH exposure. SOA mass is rapidly formed and the wall-loss-corrected mass reaches a plateau at an approximate OH exposure of $2 \times 10^7 \, cm^{-3} \, h$. In the following, comparisons between the different experiments are carried out at an OH exposure of $2 \times 10^7 \, cm^{-3} \, h$. For illustrative purposes, the wall-loss-corrected aerosol yield is shown in Fig. S8, Supplement, as a function of α-pinene reacted to demonstrate its variability between different experimental conditions.

3.1 SOA yield dependence on RH, NO_x/α-pinene and aerosol seed composition

In Figure 2, we examine the relationship between the determined yields and the prevailing experimental conditions: RH, NO_x/α-pinene and seed composition. Lines connect experiments conducted under comparable conditions, but at different RH (dashed lines) and at different NO_x/α-pinene (solid lines). The visible effects of RH and NO_x conditions on the yield in Figure 2 were statistically examined using a multilinear analysis (Fig. S9 and Table S3, Supplement). Three yield parameterizations were inter-compared and only the simplest model which represented significantly better the observations was considered for discussion.

The following features can be deduced from the analysis:

1/   SOA yields increase with α-pinene concentrations, consistent with the semi-volatile nature of SOA compounds formed. We estimate that yields increase by approximately 2 percentage points when α-pinene concentrations increase from 20 to 30 ppbv.

2/   A significant effect of the seed initial concentrations (or surface) on SOA yields was not observed. This may suggest (1) that SOA most likely forms its own phase and does not significantly partition into the seed aerosol (see below) and (2) that SOA condensation is not significantly affected by the vapor losses to the SC walls which can be diminished by increasing the aerosol surface. This is consistent with recent smog chamber results suggesting that for the α-pinene system SOA formation is dominated by quasi-equilibrium growth and vapor losses to the walls do not depend on the seed concentrations, but rather on SOA (precursor) formation (oxidation) rates (Nah et al., 2016).

3/   SOA yields are significantly reduced under high NO_x conditions (-3.3 % ± 0.6 %, p < 0.001), in agreement with literature data (Ng et al., 2007). Such a decrease indicates that SOA compounds formed under low NO_x conditions are less volatile than those formed under high NO_x conditions.

4/   We observed a clear influence of the RH on the yields, which increase on average by 1.5 ± 0.6% per 10% RH, for the range explored. This indicates that the particulate water content plays a central role in the partitioning of SOA compounds, either by altering the thermodynamic properties of the bulk phase (e.g. increasing the absorptive mass or decreasing the compound activity coefficients, non-reactive uptake) or by providing a reactive sink for semi-volatile species (e.g. formation of lower volatility compounds/oligomers in the bulk phase, reactive uptake). Additionally, the multilinear analysis suggests that the magnitude of the RH influence on SOA depends on the seed chemical nature (yields correlate with the interaction term between RH and seed composition), with a greater influence for the acidic seed (0.21 ± 0.03% per 1% RH, p < 0.001), the most hygroscopic aerosol, compared to the non-acidic seed (0.15 ± 0.03% per 1% RH, p < 0.001) and the hydrophobic seed (0.09 ± 0.04% per 1% RH, p = 0.05).

Overall, these results highlight the sensitivity of SOA yields to the prevailing oxidation conditions and the particle bulk-phase composition and water content and therefore the need for considering such conditions to obtain an accurate prediction of the SOA burden in the atmosphere. Nonetheless, results from this analysis should be regarded with some level of caution, owing to the limited size of the dataset. Despite the methodical

5   assessment of the significance of the multilinear analysis results, we cannot unambiguously propose a mechanism by which water and seed hygroscopicity/acidity enhance SOA yields nor determine whether there is interplay between these two parameters. Nevertheless, we provide evidence that both of these parameters play a significant role in the formation or condensation of SOA species. In Sect. 4, using phase partitioning computation and AIOMFAC, we shall assess to which extent and under which conditions particulate water may

10 alter the organic species' activity coefficients and as a consequence their absorptive partitioning.

3.2   SOA elemental composition

The effect of the experimental conditions on SOA chemical composition was investigated using the Van Krevelen space (Figure 3a). The overall region of the experimental data is very comparable for all experimental conditions and comparable to ambient data (Ng et al., 2011a). Data for experiments 1-14, with inorganic seeds,

15 follow a similar slope with aging (-0.84): An increase in O:C during aerosol aging takes place under all conditions. The O:C and H:C ratios of SOA produced with hydrophobic seed aerosol (expts. 15-17) show lower values than with inorganic seeds.

In Figure 3b, data are separated according to the wall-loss-corrected organic mass concentrations C_{OA} (left panel: 2–6 µg m^{-3}; middle panel: 8–14 µg m^{-3}; right panel: 16–30 µg m^{-3}), to isolate the NO$_x$ and RH effects on the

20 chemical composition from the possible influence of enhanced partitioning of semi-volatile organic species to the aerosol phase due to a higher SOA loading (Pfaffenberger et al., 2013). We observe that NO$_x$ levels have the highest influence on SOA elemental composition; namely, SOA formed at low NO$_x$ (marked with asterisks) is characterized by a higher H:C than that formed at high NO$_x$. This is even more pronounced at an early reaction stage (OH exposure $< 2 \times 10^6$ cm^{-3} h, not shown in Figure 3), where fresh SOA products formed during all low

25 NO$_x$ experiments have a higher H:C and lower O:C. Such influence of NO$_x$ levels on SOA elemental composition is consistent with our general understanding of gas-phase chemistry: Under low NO$_x$, substantial amounts of hydroperoxides and alcohols would result in a higher H:C ratio than e.g. carbonyls formed under high NO$_x$ conditions (Atkinson, 2000). Also, as hydroperoxides and alcohols are substantially less volatile than carbonyls and less fragmentation is expected at lower NO$_x$ conditions, less oxygenated species with higher

30 carbon number may partition to the particle phase at low NO$_x$, which would lead to lower O:C ratios.

NO$_x$ levels also affect the amount of organonitrate formed. Assuming that the entire nitrate signal arises from organonitrates (i.e. a maximum organonitrate contribution), we estimate molar ratios (Fig. S10, Supplement) of NO$_3$ to carbon of ~1:30 for high NO$_x$ and ~1:100 for low NO$_x$. Assuming oxidation product molecules with 10 carbon atoms, these ratios imply that every 3rd and every 10th molecule contains one NO$_3$ functional group, for

35 high and low NO$_x$ conditions, respectively.

Conversely, we could not observe a significant effect of RH and seed composition on SOA elemental composition and degree of oxygenation, despite their significant influence on SOA yields. This may be due to the limited range of O:C ratio spanned by the different experiments in our case (on average $O:C \in [0.56 - 0.75]$ at an OH exposure of 2×10^7 cm^{-3} h). Furthermore, we did not observe any significant dependence between

these parameters and the ratio of organic fragments larger than m/z 150 to the total organic mass, a proxy for oligomers measured with the HR-ToF-AMS, which would explain the observed increase in yields with the aerosol liquid water content (Fig. S11, Supplement).

3.3 Analysis of aerosol size-resolved chemical composition

5   As the seed composition and particulate water content appear to greatly influence SOA yields, we examine in this section the interaction between these parameters and SOA, through the investigation of the aerosol size-resolved chemical composition. This information is used later to infer the behavior of the absorptive organic phase and its mixing with the inorganic seed, while modeling the aerosol dynamics in the SC is beyond the scope of this study. Figure 4 shows the aerosol size resolved chemical composition at 0×10^7 cm^{-3} h, $(0.5 \pm 0.2) \times 10^7$ cm^{-3} h, $(1.0 \pm 0.3) \times 10^7$ cm^{-3} h and $(2.0 \pm 0.5) \times 10^7$ cm^{-3} h OH exposure for five experimental conditions (Data for additional experiments are available in the Supplement, Fig. S12). Figure S13 in the Supplement shows a 3-dimensional representation of the time dependent number and volume size distributions, measured by the SMPS.

For all experiments, the aerosol size distributions show two externally mixed aerosol populations, with a mode at lower diameters (~200 nm, mode 1) mostly containing SOA and another mode at higher diameters (~400 nm, mode 2) mostly consisting of the seed. We note that the particle size distribution evolved consistently under different conditions, with the smallest seed particles growing with SOA condensation or coagulation (Fig. S12 and S13, Supplement). While we have detected an increase in particle number (Fig S14, Supplement), we note that intense nucleation events did not occur. For higher yields, the main SOA mass occurs in mode 1 and despite the sizeable increase of the yield with particulate water content (e.g. under acidic conditions and high RH), we did not observe a significant enhancement of SOA in mode 2. In addition, we did not note any statistically significant correlation between the initial seed volume and SOA yields; instead SOA growth seems to be driven by the favorable partitioning of semi-volatile species to smaller particles at an early stage of the experiment (Figure 4). Such behavior would imply that semi-volatile compounds do not additionally partition or react in the electrolyte rich phase on the timescale of this experiment, but rather the reactive or non-reactive uptake of these products onto the particles is enhanced with the increase of the initial particulate water content.

3.4 Prevalent oxidation reagent and its influence on SOA yields and chemical composition

Based on the mixing ratios of OH and ozone, we estimate that a greater part of α-pinene has reacted with OH (on average 0.78 ± 0.07). Moreover, it is worthwhile to mention that the further processing of the first generation products – which do not contain C=C bonds – would almost exclusively proceed through OH oxidation. Accordingly, we conclude that SOA compounds detected are mainly from OH chemistry, independent of the NO$_x$ level and relative humidity.

We note that the fraction of α-pinene that reacted with OH under low RH (0.79 ± 0.07) and high RH (0.77 ± 0.07) are not statistically different (t-test, $p=0.71$), within our experimental variability. Therefore, we do not expect that differences in SOA yields observed between experiments at low and high RH to be due to a change in the prevalent oxidant. We recognize that water vapor may change the oxidation product distributions, via its reaction with the stabilized Criegee intermediates, produced upon the ozonolysis of α-pinene. However, we note that not only the fraction of α-pinene that reacts with O$_3$ is not substantial (in comparison with that reacted with OH), but also a major fraction of α-pinene Criegee intermediates undergoes unimolecular decomposition to form

OH and does not react with water (Atkinson and Arey, 2003). Therefore, it is unlikely that a change in RH would sizably modify the distribution of the products formed via gas-phase chemistry.

By contrast, the fraction of α-pinene that reacted with OH is found to be sensitive to the NO_x concentration. The production of O_3 was faster under high NO_x (average $[O_3]$ = 35 ppb) compared to low NO_x (average $[O_3]$ = 22 ppb), due to an efficient VOC-NO_x catalytic cycle. Consequently, the fraction of α-pinene that reacted with OH under high NO_x (0.75 ± 0.06) is lower than that under low NO_x (0.83 ± 0.04). These small, but statistically significant differences (8 percentage points; t-test, *p*=0.004) in the contribution of ozone/OH to α-pinene oxidation are expected to explain a small part of the differences in SOA yields and chemical composition observed at low and high NO_x, with higher fraction of ozonolysis products under high NO_x conditions. Despite this, we expect the influence of NO_x on the fate of RO_2 to be the main driver behind the observed differences in SOA yields and chemical composition between low and high NO_x conditions (because ozonolysis products are only a minor fraction and differences between the two conditions are rather small).

4   Phase partitioning calculation results

The organic yields and O:C ratios of the phase partitioning calculations are presented in Figure 7 and Figure 8, respectively, and listed in Table S9 of the Supplement. Each panel in Figure 7 compares organic yields for the cases org, id, sd, sdfr, and orgfr at the actual RH of the experiment (full color) and at the lower/higher RH of the corresponding experiment (light color). Table 2 gives the increase of organic yields from low to high RH of corresponding experiments as ratios [org yield (high RH) / org yield (low RH)].

The main objectives of the phase partitioning calculations are (1) estimating the impact of liquid water on SOA mixing properties (activity coefficients and liquid-liquid phase separation (LLPS)) and (2) determining the conditions or the potential model mixtures that can explain the observed yields and O:C ratios and their variation with RH. We note that model results are highly sensitive to the surrogates assumed, and the determination of SOA composition on a molecular level would considerably help confirming our results. Nevertheless, fitting both organic yields and O:C ratios significantly aid constraining the type of compounds that participate in partitioning (i.e. from a compound O:C ratio and vapor pressure its carbon number can be inferred). For example, highly oxygenated compounds cannot be very volatile without significant fragmentation, whereas oligomerization leads to a significant decrease in the compounds' vapor pressure without necessarily increasing their O:C ratios.

4.1   Simulations with reported α-pinene photooxidation products (cases org, id, sd)

For case org, the contribution of model compounds ($\chi_{j,i}$) to the volatility bins at the actual RH could be optimized such that agreement was achieved between measured and calculated yields with deviations of less than 10 %, constituting a proof of concept of the applied approach. For most simulations, the $\chi_{j,i}$-values optimized for case org were also valid for cases id and sd.

In general, simulations assuming cases org, id and sd failed in predicting the change in SOA yields with RH (Figure 7) and led to a significant underestimation of the SOA O:C ratios (Figure 8). The only exception is the pair of experiments 10/12 performed at low NO_x (1.9 ppbv) and high α-pinene levels (30.4 ppbv) for which the model could account for 87-99 % of the increase in SOA yield from low to high RH. This agreement was

achieved although the model underestimated the O:C ratios by 24 % and predicted a smaller increase in the O:C values with RH than observed. The modelled O:C remained almost constant at 0.45-0.48 at low and high RH (difference of 6 %), while the measured O:C increased from 0.56 at low RH to 0.64 at high RH (change of 14 %). We also note that the use of the more recent parameterization by Canagaratna et al. (2015) would yield
5   even higher O:C values, widening the gap between measured and modelled O:C ratios.

For the other experiments performed under low NO_x conditions, model simulations accounted for only 43-75 % of the observed yield increase with RH. Simulated O:C values ranged from 0.48 to 0.55 and failed to reproduce the observed increase from 0.57 to 0.62 for experiments 8/13 and from 0.6 to 0.64 for experiments 7/11. Likewise, for high NO_x conditions, model simulations for experiments 1/5, 2/5 and 9/14 could only account for
10   24-39 % of the observed yield increase from low to high RH and for 49-65 % for experiments 3/4. Simulated O:C values remained almost constant at 0.49-0.54 for all high NO_x experiments and were considerably lower than the observed O:C ratios.

For case id the increased SOA yield at high RH, attributed to the additional partitioning of semi-volatile compounds (norpinic acid, 2-hydroxyterpenylic acid, 10-oxopinonic acid and 4-oxopinonic acid) is a direct
15   consequence of the increased absorptive mass due to the higher water content. For cases org and sd, partitioning to the condensed phase is reduced compared to the case id as AIOMFAC predicts activity coefficients greater than 1 for higher volatility compounds, e.g. 10-oxopinonic acid and 4-oxopinonic acid. This effect is even enhanced for case sd when partitioning to the total condensed phase including the seed aerosol is simulated. Although LLPS is predicted for all simulations, the salting-out effect of AS which partitions to some degree also
20   to the organic phase leads to a further decrease of the organic yield at high RH compared to the case id.

In summary our results suggest that with the reported model compounds for α-pinene photooxidation, the measured O:C and the increase of organic yields with RH cannot be simulated. Therefore, we explored whether the formation of fragmented and more oxidized products may explain the high O:C ratio observed and the high sensitivity of the yields to RH.

25   **4.2   Simulations including fragmented products (cases sdfr and orgfr)**

Non-fragmented products (e.g. highly oxygenated C10 or dimers) would be low-volatility (LVOC) or extremely low-volatility organic compounds (ELVOC) (Zuend and Seinfeld, 2012; Donahue et al., 2006; 2012b) with effective saturation concentrations $C^* \leq 0.1$ µg m^{-3}, when their O:C ratio is as high as the observed O:C ratio. Therefore, they are expected to be in the particle phase independent of the prevalent RH and the inclusion in the
30   model of additional amounts of these products would not help explaining the observed difference in the yields at different RH, leading to an overestimation of OA mass at low RH. This implies that to better capture the measured O:C range without overestimating SOA yields, fragmented products with shorter backbones need to be introduced.

Low molecular weight compounds resulting from fragmentation were therefore added to the volatility bins with
35   $C^* = 1\text{-}100$ µg m^{-3}, namely, 3-oxoadipic acid to the volatility bin with $C^* = 1$ µg m^{-3}, glutaric acid to the volatility bin with $C^* = 10$ µg m^{-3} and 5-COOH-3-OH-pentanal and succinic acid to $C^* = 100$ µg m^{-3}. For case sdfr, α_i-parameters were optimized assuming equilibrium partitioning of SOA to the whole condensed phase including the seed aerosol. For case orgfr absorption to the organic phase only was assumed. While the organic and the inorganic phases seem to form externally mixed particles based on the chemically resolved size

distribution, examining both cases provides valuable insights into the impact of the presence of an inorganic aerosol seed in the system. Tables S7 and S8 of the Supplement provide the contribution of model compounds ($\chi_{j,i}$ values) to volatility bins C_i^* for these cases. The organic yields and O:C ratios for cases sdfr and orgfr are shown in Figure 7 and Figure 8, respectively. In Table 2 the relative increase in SOA yields from low to high RH is given. Cases sdfr and orgfr are similarly successful in reproducing SOA yields and O:C ratios. However, the variability in the modelled yields when using different volatility distributions for cases sdfr and orgfr is larger than for cases org, id, and sd (Figure 7).

For experiments carried out at low NO_x conditions (experiments 7/11, 8/13 with NO_x < 2 ppbv), both cases explained the observed increase in the organic yields with RH and improved the agreement between modelled and observed O:C ratios. For experiments 8/13, both cases accurately captured the increase in SOA yields from low to high RH with deviations < 2 %. Modelled O:C agreed very well with measurements for case sdfr with deviations ≤ 1% and slightly worse for case orgfr with deviations of ≤ 5%. For experiments 7/11, cases sdfr and orgfr reproduced satisfactorily (deviations ≤ 11%) the measured yields for calculations with the volatility distributions determined for experiment 11, but overestimated the observed increase of O:C from low (O:C = 0.60) to high RH (O:C = 0.64). Using the volatility distributions determined for experiment 7, the low yields at low RH could not be achieved. For experiments 10/12, cases org, id, and sd were able to simulate the increase of organic yield with the oxidation products reported in literature but failed to reproduce the observed O:C ratios. Cases sdfr and orgfr with additional oxidized and fragmented products showed improved agreement of observed yields and reproduced successfully the observed O:C ratios.

Under high NO_x conditions, cases sdfr and orgfr could only simulate satisfactorily SOA yields and O:C ratios observed during experiments 3/4. For experiments 1-2/5 and 9/14, model and measurement agreement was less satisfactory. The model could not reproduce the low yields at low RH observed during experiments 5 and 14 and hence the strong reduction of the yields observed with the decrease in RH is underestimated (the simulations predict only 52-66 % of the observed change). Additionally, for these experiments the model underestimates the O:C ratios (average measured O:C = 0.66 and 0.68, at low and high RH, respectively). In the following, we examine and discuss the potential reasons that might explain model-measurements disagreements.

4.3   Simulations including organonitrates

We examined whether the discrepancy between modelled and measured yields may be ascribable to the selection of the model compounds at high NO_x, by introducing additional surrogates - specifically organonitrates - expected to be representative of the compounds formed under these conditions. Assuming that the NO_3 signal in the HR-ToF-AMS originates from organonitrates, every 3rd molecule should contain one ONO_2 functional group at high NO_x conditions. We tested whether adding organonitrates described by Valorso et al. (2011) would improve the agreement between measurements and observations for the high NO_x experiments. However, this was not the case (not shown). Such sensitivity tests could not be performed for cases including partitioning to the seed aerosol because interaction parameters between organonitrates and sulfate are not available in AIOMFAC.

4.4   Simulations including higher volatility oxidation products

The Monte Carlo simulations enabled the determination of α_i-parameters for volatility bins C^* = 0.1-100 µg m^{-3}. α_i-Parameters in the volatility bin with C^* = 1000 µg m^{-3} could not be reliably extracted. Nevertheless, SOA

products belonging to this bin are present in the chamber and could partition to some extent to the condensed phase. We investigated whether the presence of substances with an effective saturation concentration of 1000 µg m^{-3} could reproduce the low SOA yields at low RH and its strong increase at high RH observed for the high NO$_x$ experiments 1/5, 2/5, and 9/14. This was achieved by replacing a part of the substances in the volatility bin

5    $C^* = 100$ µg m^{-3} by pinalic acid, terpenylic acid and 3-2-oxopropanylolxypropanoic acid (Table S4, Supplement). While the addition of these compounds in the model could reproduce the low yields at low RH, the yields at high RH were strongly underestimated (not shown). Accordingly, the introduction of organonitrates or higher volatility compounds in the model did not improve the agreement between modelled and observed yields and O:C ratios (not shown here), suggesting that equilibrium partitioning alone cannot explain the strong SOA

10   yield increase under high NO$_x$ conditions.

4.5   Partitioning of individual components to the gas phase and condensed phases

The phase partitioning calculations do not only allow the simulation of the total organic yield and average O:C ratio of the condensed products, but also provide insights to the partitioning of individual compounds to the gas phase and the condensed phases. Phase partitioning of individual model compounds into the gas and condensed

15   phases for case sdfr is examined in Figure 9 for experiments 8/13 and in Figure 10 for experiments 3/4. Detailed results of the phase partitioning calculations are listed in Tables S10 and S11 in the Supplement. For experiments 8/13, the model predicts an LLPS into an organic-rich phase (op) and a predominantly electrolyte-like phase (ep). Overall, organic compounds are predominantly in the organic phase at both RH with ep/op $< 1 \cdot 10^{-5}$ at 25 % RH, and ep/op $\approx$ 0.003-0.008 at 60 % RH. Compounds in volatility bins $C^* = 0.01$ and 0.1 µg m^{-3} are mainly

20   present in the condensed phases, while compounds in volatility bin $C^* = 100$ µg m^{-3} show preferred partitioning to the gas phase. The strongest increase in the condensed phase when RH is increased from 25 % to 60 % is observed for the model compounds assigned to $C^* = 100$ µg m^{-3}. Moderately oxygenated species (4-oxopinonic acid and 10-oxopinonic acid) in this bin show a moderate increase (about a factor of two) driven by the increase of the absorptive mass. This increased partitioning is limited by an increase in the activity coefficients of these

25   compounds (for experiment 8 from 1.69 and 1.63 at low RH to 2.70 and 2.93 at high RH and for experiment 13 from 1.49 and 1.54 at low RH to 2.88 and 3.24 at high RH). Conversely, the 5-fold enhanced partitioning of the fragmented and more functionalized compounds (5-COOH-3-OH-pentanal and succinic acid) into the condensed phase at high RH is driven by the increase of the absorptive mass and the slight decrease of the compounds' activity coefficients (for experiment 8 from 0.84 and 0.51 at low RH to 0.68 and 0.43 at high RH and for

30   experiment 13 from 0.90 and 0.56 at low RH to 0.69 and 0.44 at high RH).

For experiments 3/4, model results obtained from the parameterization of the yields in experiment 4 are highly sensitive to the assumed volatility distribution. As shown in Figure 10, when introducing volatility distributions characterized by high contributions of semi-volatile oxygenated compounds pertaining to the volatility bin $C^* = 100$ µg m^{-3}, the model predicts a liquid phase mixing. Note that when mixing is predicted, the model tends to

35   overestimate the O:C ratio (O:C = 0.81 at high RH for the volatility distribution #2 shown in the upper panels of Figure 10) and the yields at both high and low RH. Conversely, when volatility distributions with less volatile and less oxygenated compounds are used (e.g. volatility distribution #93), lower yields and lower O:C ratios (0.69 for volatility distribution #93 shown in the lower panels of Figure 10) are obtained and LLPS is predicted. For such O:C ratios LLPS has also been observed for experiments performed with model mixtures (e.g. Song et

40   al., 2012). For experiment 4, the volume of the electrolyte phase is larger than that of the organic-rich phase and

there is considerable partitioning of organic compounds to the electrolyte phase (ep/op = 2.26). These observations illustrate that for compounds with high O:C ratios, small differences in the volatility distribution parameters can lead to totally different phase partitioning. Irrespective of these differences, none of the volatility distributions used could reproduce the measured yields at both high and low RH, likely due to the deficient

5   representation in the model of the interactions between the acidic aerosol and the organic compounds - and of the chemical processes occurring under acidic/high NO_x conditions.

4.6   Modeling considerations and limitations

Model simulations were carried out by considering two α-pinene C8-C10 photo-oxidation products per volatility bin for cases org, id and sd. This number was sufficient to represent the species within one volatility bin, because

10   the hydrophilicity of these compounds with consistently high carbon number correlates with their volatility. Therefore the sensitivity of model predictions to the contribution of these compounds to the volatility bins (described by $\chi_{j,i}$ values) is relatively low. This model setting, corresponding to a pseudo-one-dimensional VBS where the compounds' vapor pressure and degree of oxidation correlate, was proven to be insufficient for an accurate description of both SOA mass and degree of oxygenation. By contrast, for cases sdfr and orgfr, which

15   include more oxidized short chain products, hydrophilicity and volatility may be varied more independently, which introduces an additional degree of freedom and would correspond to a pseudo-two-dimensional VBS (2D-VBS), as described by Donahue et al. (2011). While we show that model predictions based on this setting are highly dependent on the volatility distribution parameters and model compounds assumed, in general the introduction of fragmented more oxidized compounds reproduced well the high observed O:C ratios and the

20   increase of O:C and SOA yields with RH, specifically at low NO_x. The estimated volatility distributions and average carbon (C~6) and oxygen (O~4) numbers when considering fragmented products are in agreement with chemical speciation analysis previously reported for the same system (Chhabra et al., 2015). The analysis shows that for such semi-volatile products with O:C ratios in the order of ~0.6 an increase of RH from 23-29 % to 60-69 % induces a mass increase by up to a factor of three, driven by the higher particle water content and the lower

25   activity coefficients of the more fragmented products at high RH.

The measured O:C ratio is a key parameter for constraining the model. Here, we have used the high resolution parameterization proposed by Aiken et al. (2007), while the use of the more recent parameterization by Canagaratna et al. (2015) would result in even higher O:C ratios (by 18 %). Higher O:C ratios would require increasing even further the contribution or the degree of oxidation of the fragmented compounds and would

30   imply that the model predicts an even higher sensitivity of the yields to RH. Therefore, the O:C values used here yield more conservative estimates of the contributions (or the degree of oxidation) of fragmented products in the model and of the sensitivity of the yields and O:C ratios to the RH.

Under high NO_x (and low pH), the model could not reproduce the factor of six increase in yields at high RH, using a variety of chemically dissimilar surrogate compounds. This indicates that the increased absorptive uptake

35   of these compounds due to the increase in SOA mass and the decrease in the compounds' activity coefficients cannot explain the observed enhancements alone. Under these conditions, additional processes may likely play a role in the enhancement of OA with RH. NO_x concentrations have a dramatic influence on SOA chemical composition and volatility. Therefore, the discrepancy between model and measured yields at high NO_x conditions may be explained by either an inadequate representation of SOA surrogates in the model and their

interaction parameters with the seed or by an enhanced reactive uptake of SOA species formed under high NO_x conditions, such as carbonyls that are reported to instigate the formation of lower volatility compounds in the particle phase (Shiraiwa et al., 2013 and references therein). Given the dearth of additional chemically resolved measurements of the particle phase species formed under different conditions, the mechanism by which RH

5   enhances the uptake of SOA species under high NO_x (low pH) remains currently undetermined.

Cases org, id, and orgfr assumed gas-particle partitioning into the organic aerosol only. In this case, the role of the seed aerosol is restricted to providing a substrate for nucleation of organic vapors. This is the case for effloresced seed particles. For liquid seed aerosols this is equivalent to a complete organic/electrolyte phase separation with no partitioning of inorganic ions to the organic phase. For cases sd and sdfr equilibrium

10   partitioning between the gas phase and the entire condensed phase including the seed aerosol is assumed leading in most cases to LLPS. The current model does not yet contain interaction parameters of bisulfate with all involved organic functional groups. Therefore, ammonium bisulfate was treated as ammonium sulfate in the model, and we are not capable of distinguishing whether the enhanced partitioning of semi-volatile vapors in the acidic medium is attributable to additional reactions in the bulk phase (catalysed at lower pH) or to an enhanced

15   solubility of SOA species.

Considering the size-resolved particle chemical composition discussed in Sect. 3.3 (Figure 4), LLPS is likely not realized within single particles but the aerosol population splits up into a predominantly organic mode at ~200 nm and a predominantly inorganic mode at ~400 nm. The formation of these two populations may occur by the homogeneous or heterogeneous nucleation of highly oxidized non-volatile products. Homogeneous

20   nucleation implies new particle formation (which would only be moderate – see Figures S13 and S14 – due to the high condensation sink in the chamber), while heterogeneous nucleation proceeds via condensational growth (which would occur on smaller particles with higher surface). Both processes are expected to create small organic rich particles, providing an organic absorptive phase into which additional semi-volatile compounds may preferentially partition. When the organic and electrolyte phases are present in different particles the two phases

25   communicate via gas phase diffusion, and equilibration time-scales depend on the components' volatility. For compounds with $C^* = 0.1$-$100\ \mu g\ m^{-3}$ equilibration occurs within time-scales of minutes to tens of minutes, assuming no bulk phase diffusion limitations (Marcolli et al., 2004). In the larger particle electrolyte-rich mode, the inorganic ions would exert a salting-out effect driving the organic compounds to partition to the gas-phase or into the smaller organic-rich particles. This would prevent the organic compounds from partitioning in

30   significant amounts into the seed aerosol from the beginning and deplete even further these larger particles from the organic material. Under such a scenario an externally-mixed phase-separated aerosol may evolve in the smog chamber. Overall, the size-resolved chemical composition information confirms the modelling results providing compelling evidence for organic-electrolyte LLPS.

The scenario outlined above is based on equilibrium partitioning and does not invoke diffusion limitations within

35   the condensed phase. Recent evidence may challenge this assumption, suggesting that SOA may adopt a highly-viscous state (e.g. Virtanen et al., 2010; Koop et al., 2011), where bulk diffusion and evaporation are kinetically limited. However, while such behavior occurs under certain conditions, e.g. low temperature and low relative humidity, we expect that this is not the case for the aerosol investigated in this study. Saleh et al. (2013) showed that SOA from α-pinene ozonolysis reaches equilibrium with the gas phase within tens of minutes at low mass

40   loadings (2-12 $\mu g\ m^{-3}$) upon a step-change in temperature. Robinson et al. (2013) determined by aerosol mixing

experiments that the diffusion coefficient in α-pinene-derived SOA is high enough for mixing on a time scale of minutes. Fast mixing is further supported by measurements of ambient OA (Yatavelli et al., 2014) showing that biogenic SOA reaches equilibrium within atmospheric time scales, under similar conditions as those in our chamber. Therefore, we expect that, if thermodynamically favorable, liquid-liquid mixing would have occurred

5   under the time-scales of our experiments and a unimodal particle population would have emerged. However, consistent with model predictions, this is not the case.

5   Summary and conclusions

We conducted a series of smog chamber experiments to investigate the impact of NO_x/VOC ratios, RH and the seed aerosol composition on the yield and the degree of oxygenation of SOA produced from α-pinene

10   photooxidation. We developed a novel approach based on Monte Carlo simulations to determine SOA volatility distributions from the measured yields using the volatility basis set framework. Measured yields spanned an order of magnitude (2-20 %), depending on the prevailing oxidation conditions, the particle bulk-phase composition and the water content. This underlines the need of considering these conditions for an accurate prediction of the SOA burden in the atmosphere. The yields increased dramatically with RH, aerosol acidity and

15   at low NO_x. The aerosol bulk chemical composition measured by the HR-ToF-AMS appears to be mostly dependent on NO_x/VOC ratios.

We investigated whether equilibrium partitioning between the gas and the condensed phase(s) can reproduce the measured SOA yield and O:C ratio at low and high RH. For this, the thermodynamic group-contribution model AIOMFAC was used to examine the partitioning of a range of selected surrogate compounds with different

20   volatilities and O:C ratios as a function of their activity coefficients and the particle water content; properties that are altered with the variation of RH. In practice, two to four surrogate compounds were assigned to each volatility bin based on the volatility distributions derived from experimental data and the compounds' effective saturation concentration, which depends on the pure component saturation vapor pressures. The RH was then varied in the model and changes in SOA mass and O:C ratios were monitored. There are large discrepancies

25   between vapor pressures determined for semi-volatile and low volatility compounds depending on the measurement techniques (Huisman et al., 2013; Bilde et al., 2015), which introduce inaccuracies in saturation vapor pressure estimations. However, these uncertainties do not affect the approach applied in this study because an incorrect assignment of a model compound to a volatility bin does not change the experimentally derived volatility bin distribution. The share of the individual model compounds to the volatility bins was used as fitting

30   parameter to achieve agreement between measurements and calculations. In addition, as a set of volatility distribution functions was obtained for each experiment through the Monte Carlo simulations, the approach is proven very effective in assessing the sensitivity of equilibrium partitioning calculations on the volatility distribution input parameters.

Our results show that only with the inclusion of fragmentation products the model could simultaneously explain

35   SOA concentrations and O:C ratios. Under these conditions, the model predicts that an increase in RH from ~25 % to ~60 % may lead to a three-fold enhancement in SOA mass, due to the increase in the absorptive mass and the slight decrease in the compounds' activity coefficients. While the magnitude of this increase is consistent with the experimental observation at low NO_x, equilibrium partitioning alone could not explain the strong increase in the yields with RH observed for the high NO_x experiments (factor ~6). This suggests that other

processes including the reactive uptake of semi-volatile species into the liquid phase may occur and be enhanced at higher RH, especially for compounds formed under high NO_x conditions such as carbonyls. Future studies should investigate the dependence of SOA compounds on RH, NO_x and aerosol acidity at a molecular level. Such measurements shall provide additional insights into the chemical nature of the compounds that additionally partition or react at higher RH and also the mechanisms via which such processes occur.

For most of the cases studied, the model predicts liquid-liquid phase separation into an organic and an electrolyte phase. Considering the size-resolved particle chemical composition, this phase separation is likely not realized within single particles but the aerosol population splits up into a predominantly organic mode at ~200 nm and a predominantly inorganic mode at ~400 nm. Based on our results, such liquid-liquid phase separation is expected to occur under most ambient conditions, i.e. similar levels of OA and sulfate, O:C < 0.8, and RH < 70–80 %.

Acknowledgements. This work has been supported by the EU 7th Framework projects EUROCHAMP-2 and PEGASOS, as well as the Swiss National Science Foundation (Ambizione PZ00P2_131673, SAPMAV 200021_13016), the EU commission (FP7, COFUND: PSI-Fellow, grant agreement n.° 290605) and the joint CCES-CCEM project OPTIWARES. We thank René Richter and Günther Wehrle for their technical support at the smog chamber, and in addition Michel J. Rossi, Martin Gysel, Neil Donahue and Barbara Turpin for the helpful discussions. We thank Andreas Zuend for providing the Fortran code for phase partitioning calculations and AIOMFAC and helpful discussions.

6   Tables and Figures

Table 1. Overview of experimental conditions. Seed types {AHS = ammonium hydrogen sulfate (NH_4HSO_4); SA = sulfuric acid (H_2SO_4); AS = ammonium sulfate (($NH_4)_2SO_4$); CF = fluorinated carbon (see Sect. 2.2)} and their assumed phase states: (L) = liquid; (-) = liquid and/or solid. Initial seed mass concentrations; relative humidity (RH); measured mean NO_x concentrations during low NO_x experiments (marked with an asterisk*) and measured initial NO_x concentrations during high NO_x experiments; measured initial α-pinene concentrations (which reacted before an OH exposure of $(2.0 \pm 0.5) \times 10^7$ cm^{-3} h) and their estimated fractions reacted with OH radicals in %, rest reacted with O_3). NO_x/α-pinene ratios; wall-loss corrected organic mass concentrations (C_{OA}) and corresponding yields Y averaged over the OH exposure of $(2.0 \pm 0.5) \times 10^7$ cm^{-3} h. Standard deviations (1sd) given in brackets are measurement variability. Horizontal lines separate experiments with different i) seed composition, ii) RH, iii) NO_x/α-pinene. Blank experiments (B1, B2 and B3) are listed at the very bottom.

No	seed type (phase)	initial	RH	NO_x initial or mean(*)	α-pin initial = reacted	α-pin decay by OH	NO_x/ α-pin	C_{OA} (wlc) at OH exposure: $(2.0\pm0.5) \times 10^7$ cm^{-3} h	Yield, Y (wlc)
		µg m^{-3}	%	ppbv	ppbv	%		µg m^{-3}	
1	AHS+SA (L)	8.0(0.5)	69(2)	44.4(0.8)	20.7	80.0	2.1	13.4(0.2)	0.115
2	AHS+SA (L)	12.3(0.5)	67(2)	70.4(1.3)	18.7	80.3	3.8	8.6(0.1)	0.081
3	AHS+SA (L)	4.9(0.3)	66(2)	19.6(0.7)	16.1	81.6	1.2	12.6(0.6)	0.138
4	AHS+SA (L)	4.7(0.2)	29(1)	23.6(0.6)	19.9	81.3	1.2	3.9(0.0)	0.035
5	AHS+SA (L)	8.0(0.3)	28(1)	52.1(0.6)	20.3	74.6	2.6	2.1(0.1)	0.018
6	AHS+SA (L)	5.2(0.3)	27(1)	1.3(0.4)*	18.3	87.8	0.071	12.0(0.5)	0.116
7	AS+AHS (L)	8.8(0.4)	67(1)	0.7(0.2)*	20	81.9	0.037	16.2(0.4)	0.143
8	AS+AHS (L)	4.3(0.6)	60(1)	1.0(0.2)*	18.7	86.5	0.052	12.3(0.4)	0.116
9	AS+AHS (L)	5.5(0.2)	56(2)	65.8(0.8)	30.9	65.0	2.1	11.1(0.1)	0.064
10	AS+AHS (L)	4.4(0.2)	50(1)	1.3(0.2)*	30.6	79.2	0.041	29.6(1.1)	0.171
11	AS+AHS (-)	4.1(0.2)	26(1)	0.7(0.3)*	18.9	81.3	0.039	5.5(0.2)	0.051
12	AS+AHS (-)	3.6(0.1)	26(1)	1.9(0.4)*	30.5	78.4	0.062	20.3(1.3)	0.118
13	AS+AHS (-)	8.2(0.3)	25(1)	1.1(0.3)*	19.6	87.4	0.055	5.3(0.1)	0.048
14	AS+AHS (-)	3.2(0.2)	23(1)	75.1(0.7)	27.8	69.4	2.7	2.4(0.1)	0.015
15	CF (L)	7.1(0.3)	58(1)	56.2(0.7)	31.7	67.9	1.8	9.8(0.1)	0.054
16	CF (L)	10.0(0.5)	58(2)	58.3(0.5)	31.3	73.9	1.9	10.7(0.1)	0.061
17	CF (L)	6.7(0.1)	26(1)	53.3(0.6)	30.5	69.7	1.7	4.7(0.1)	0.021
B1	CF (L)	0.3(0.1)	58(2)	53.0(0.6)	-	-	-	< 0.1	-
B2	AS+AHS (L)	4.5(0.7)	68(2)	0.9(0.5)*	-	-	-	2.8(1.0)	-
B3	AHS+SA (L)	3.8(0.2)	75(3)	1.4(0.3)*	-	-	-	0.5(0.1)	-

Table 2. Increase of organic yield from low to high RH for the different experiments as org yield (high RH) /org yield (low RH). The second column lists the ratio of measured organic yields enhancements with RH. In the five last columns the ratios of organic yields calculated at high and low RH for the different experiments are given (average value of the ten volatility distributions with lowest and highest values in brackets in the second row).

Experiments		Calculations					
Expt. No.	yield ratio	Exp	Case org	Case id	Case sd	Case sdfr	Case orgfr
1 / 5	6.38	1	1.62 (1.48-1.86)	2.02 (1.67-2.57)	1.54 (1.37-1.77)	4.23 (2.50-6.70)	4.34 (2.89-6.62)
2 / 5	4.10	2	1.42 (1.23-1.47)	1.61 (1.31-1.73)	1.31 (1.18-1.35)	2.74 (1.33-6.24)	2.24 (1.35-2.92)
3 / 4	3.23	3	1.64 (1.44-1.86)	2.07 (1.88-2.38)	1.57 (1.48-1.73)	3.67 (2.74-5.29)	3.13 (2.53-4.14)
3 / 4	3.23	4	1.76 (1.58-1.90)	2.09 (1.78-2.41)	1.58 (1.44-1.71)	2.93 (1.91-4.88)	3.12 (2.13-4.09)
7 / 11	2.95	7	1.35 (1.25-1.47)	1.52 (1.35-1.80)	1.28 (1.20-1.39)	2.16 (1.48-3.98)	2.38 (1.64-3.69)
8 / 13	2.32	8	1.43 (1.30-1.58)	1.61 (1.43-1.87)	1.36 (1.27-1.50)	2.66 (1.60-4.79)	2.44 (1.73-3.57)
9 / 14	4.63	9	1.43 (1.32-1.59)	1.56 (1.38-1.82)	1.33 (1.23-1.48)	2.45 (1.61-4.70)	2.69 (1.75-4.24)
10 / 12	1.46	10	1.29 (1.13-1.52)	1.38 (1.22-1.67)	1.28 (1.17-1.49)	1.44 (1.18-1.66)	1.55 (1.26-2.17)
7 / 11	2.95	11	1.80 (1.52-2.21)	2.22 (1.69-3.09)	1.67 (1.40-2.05)	2.74 (1.75-4.03)	3.38 (1.87-5.61)
10 / 12	1.46	12	1.34 (1.21-1.48)	1.48 (1.27-1.71)	1.33 (1.19-1.49)	1.34 (1.19-1.65)	1.70 (1.33-2.06)
8 / 13	2.32	13	1.54 (1.39-1.68)	1.74 (1.52-1.91)	1.41 (1.30-1.50)	2.73 (1.29-6.06)	2.54 (1.39-4.90)
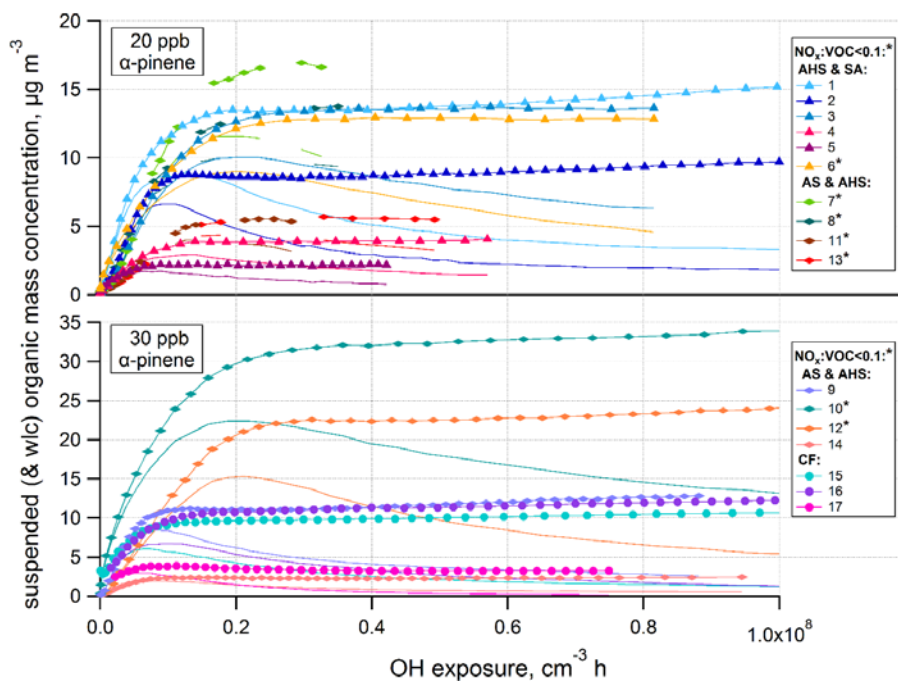
Figure 1. 20-min-averaged wall-loss-corrected (symbols & lines) and suspended (lines) organic mass concentrations as a function of OH exposure. Data is separated according to similar initial α-pinene concentration (20 ppbv - top panel, 30 ppbv - bottom panel). Experiment numbers are given in the legend and classified by seed composition; asterisks indicate low NO_x experiments.
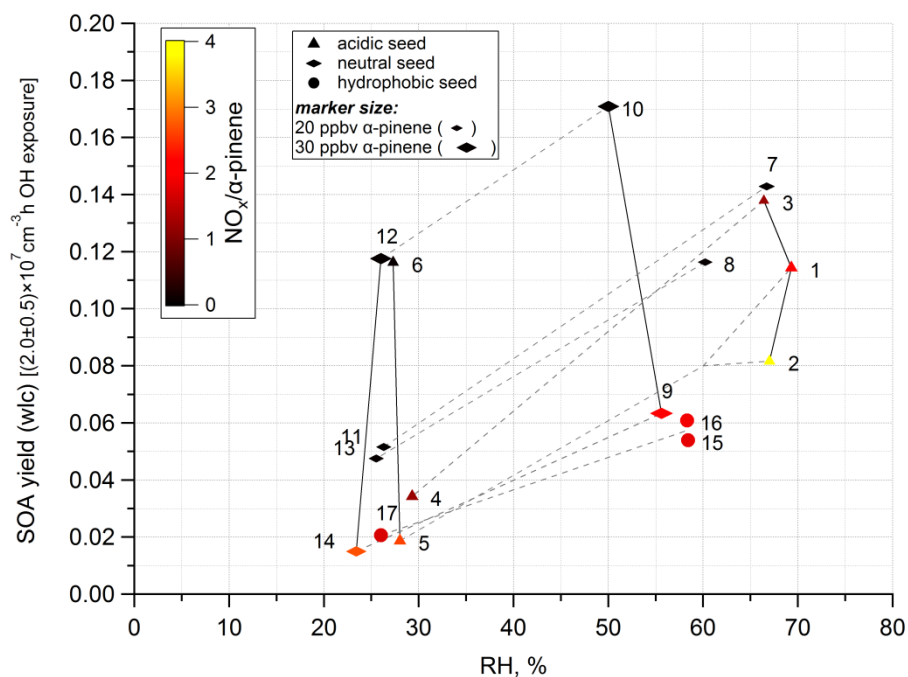
Figure 2. Average wall-loss-corrected yields Y at $(2.0 \pm 0.5) \times 10^7$ cm^{-3} h OH exposure as a function of RH. Symbol sizes represent α-pinene reacted, symbol colors represent NO$_x$/α-pinene and symbol shapes represent seed composition according to Table 1. Experiments with similar NO$_x$/α-pinene, seed composition and α-pinene reacted are connected with dashed lines showing the increase in yield for increased RH. Experiment 6 has no counterpart experiment at high RH. Experiments with similar RH, α-pinene reacted and seed composition are connected with solid lines showing the increased yield with decreasing NO$_x$/α-pinene ratio.
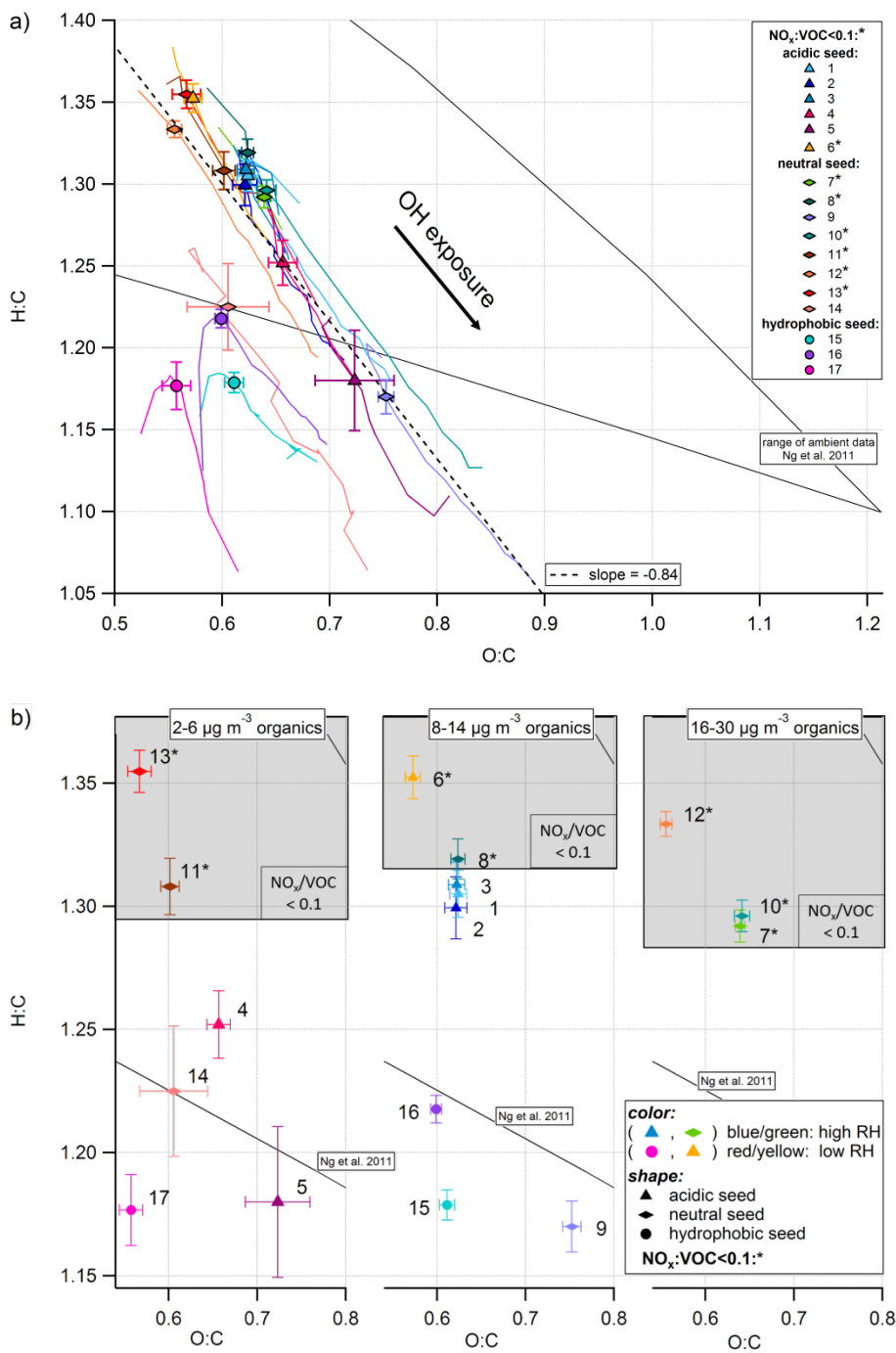
Figure 3. Van Krevelen diagrams: Mean (and 1 standard deviation measurement variability) H:C versus O:C at OH exposure $(2.0 \pm 0.5) \times 10^7$ cm^{-3} h (symbols). Symbol colors indicate RH, symbol shapes the seed composition and the asterisk low NO$_x$ experiments. (a) The dashed line represents the (least orthogonal distance) fitted slope of experiments (1-14) with inorganic seed: -0.84. The triangular shaped solid lines) represents the range of ambient SOA (Ng et al., 2011a). 1 h-averages of H:C versus O:C (for OH exposure > 2×10^6 cm^{-3} h) are given by the colored lines. Experiments 15-17 show the influence of organic seed compounds (data shown from suspended organic mass > 0.3 µg m^{-3}). (b) The data was split in three groups according to their wall-loss-corrected organic mass concentrations to exclude concentration effects (left panel: 2-6 µg m^{-3}; middle panel: 8-14 µg m^{-3}; right panel: 16-30 µg m^{-3}). The grey shaded areas include all low NO$_x$ experiments.

a)

b)
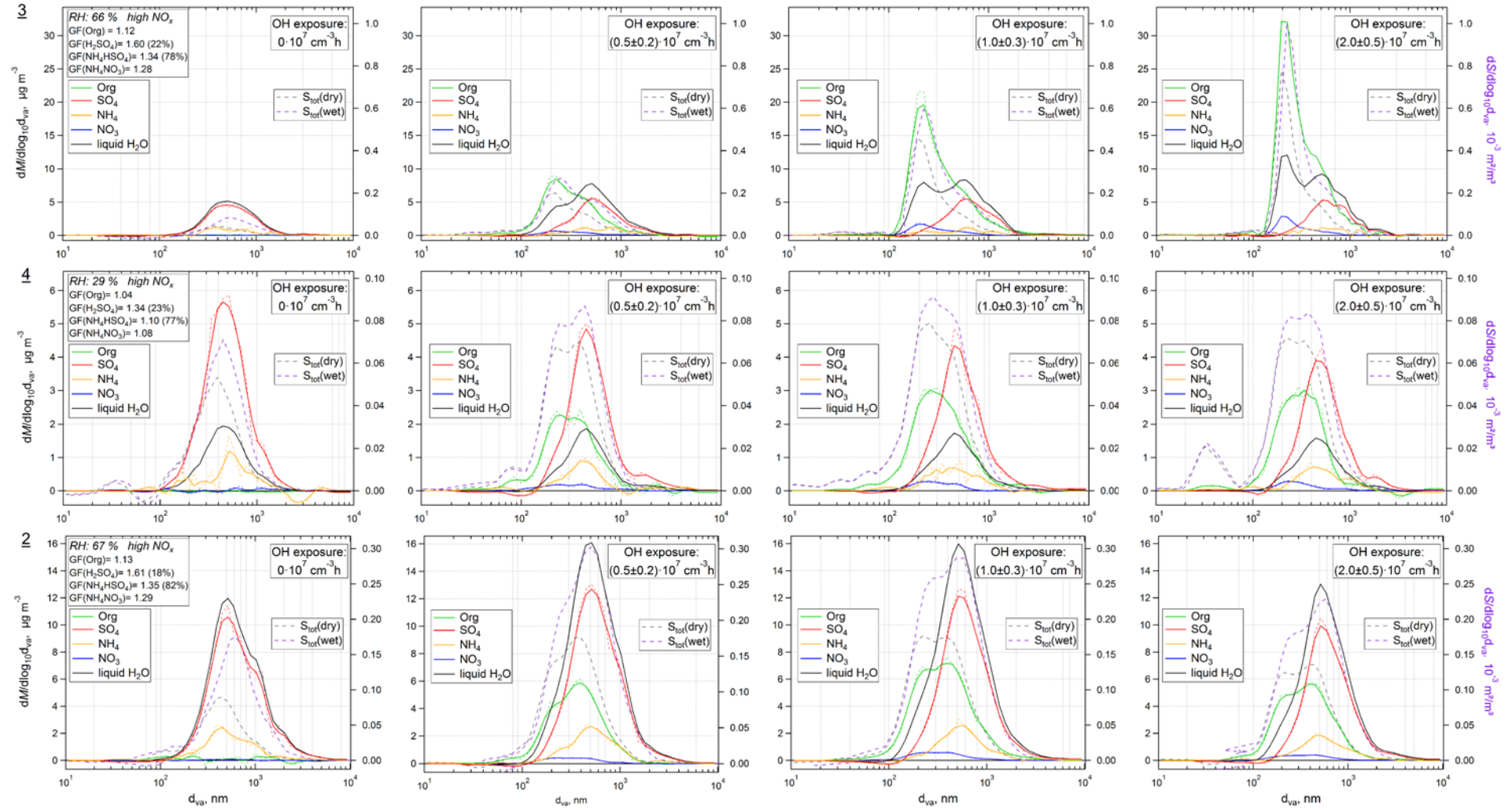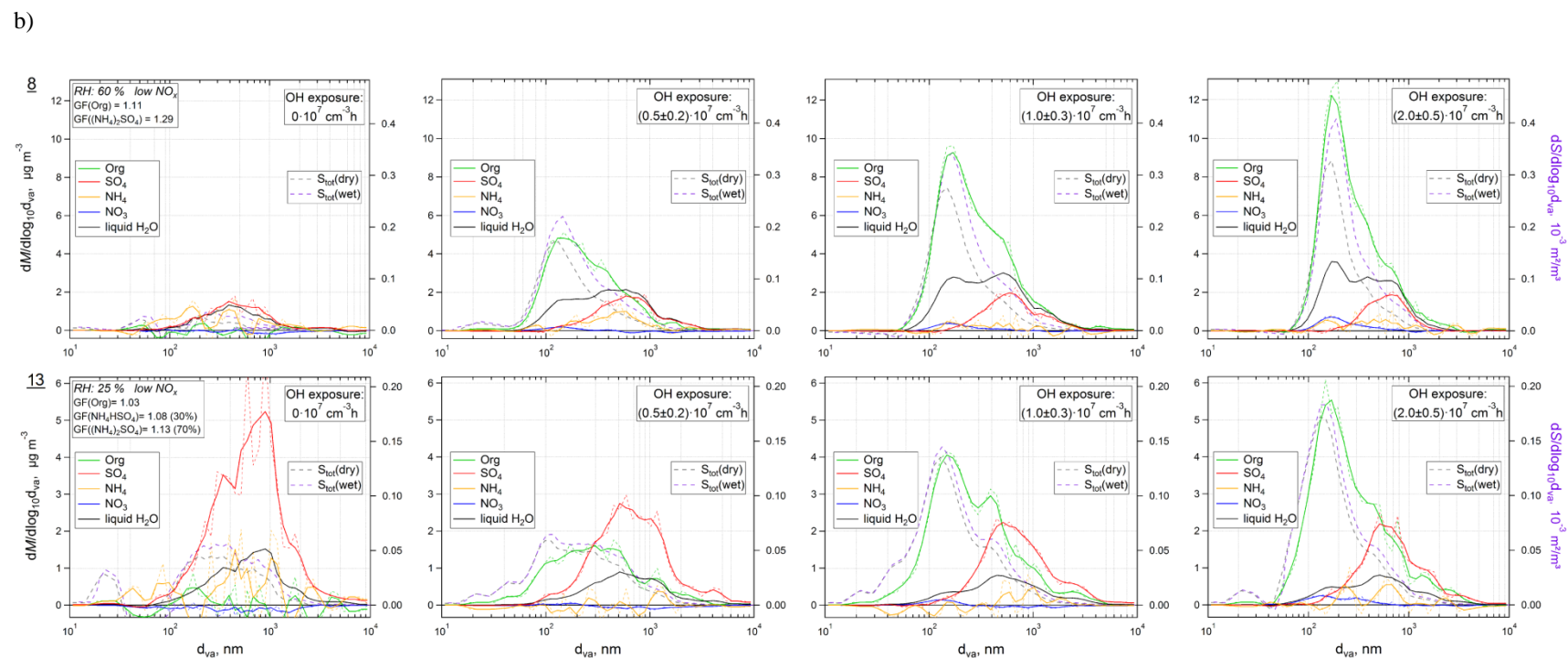
Figure 4. Evolution of size distributions from the HR-ToF-AMS. Measured organic, SO₄, NH₄, NO₃ mass distributions for OH exposures of 0×, (0.5 ± 0.2)×, (1.0 ± 0.3)× and (2.0 ± 0.5) × 10⁷ cm⁻³ h. Black lines represent estimated liquid water content (method: Sect. 2.3; RH and individual *GF*s given in the legend, percentage in brackets: fractions of SO₄). The calculated dry and wet surface distributions are shown as dashed lines on the right axes. (a) High NOₓ with more acidic seed [H₂SO₄ & NH₄HSO₄]: Experiments 3 and 4 with NOₓ/α-pinene = 1.2 and experiment 2 with NOₓ/α-pinene = 3.8. (b) Low NOₓ with less acidic seed [(NH₄)₂SO₄ & NH₄HSO₄]: Experiments 8 and 13 with NOₓ/α-pinene ≈ 0.05. Additional figures in the Supplement (Fig. S12).
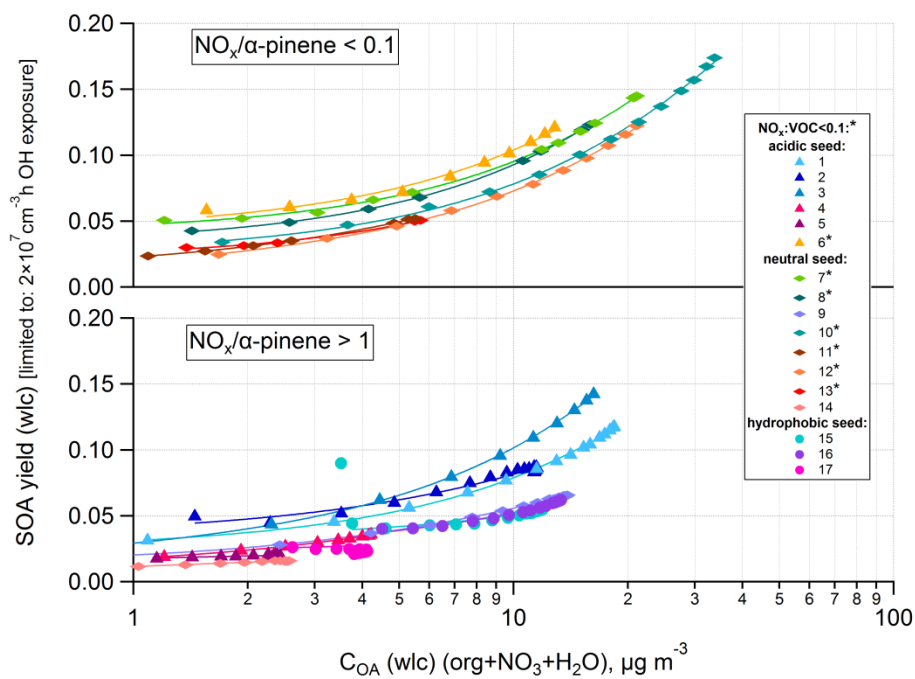
Figure 5. Measured (symbols) and parameterized (lines) wall-loss-corrected SOA yield, *Y*, as a function of wall-loss-corrected absorptive mass concentration (C_{OA}: organics + NO$_3$ + H$_2$O) for low NO$_x$ experiments (upper panel) and high NO$_x$ experiments (lower panel). Data was limited to an OH exposure of 2×10^7 cm^{-3} h and averaged over 20 minutes. Symbol colors indicate the RH, symbol shapes the seed composition and the asterisks the NO$_x$/VOC ratio.
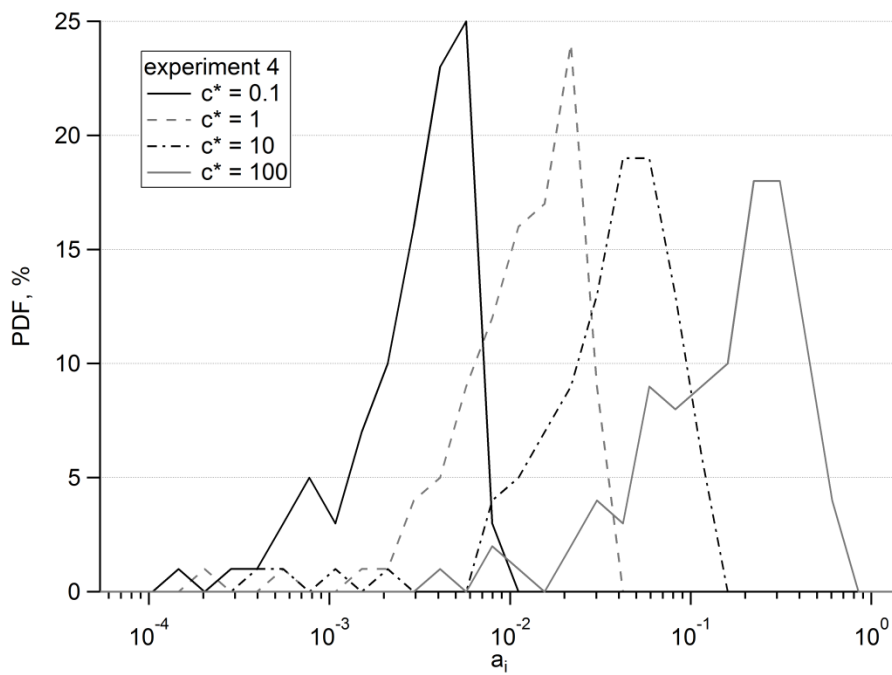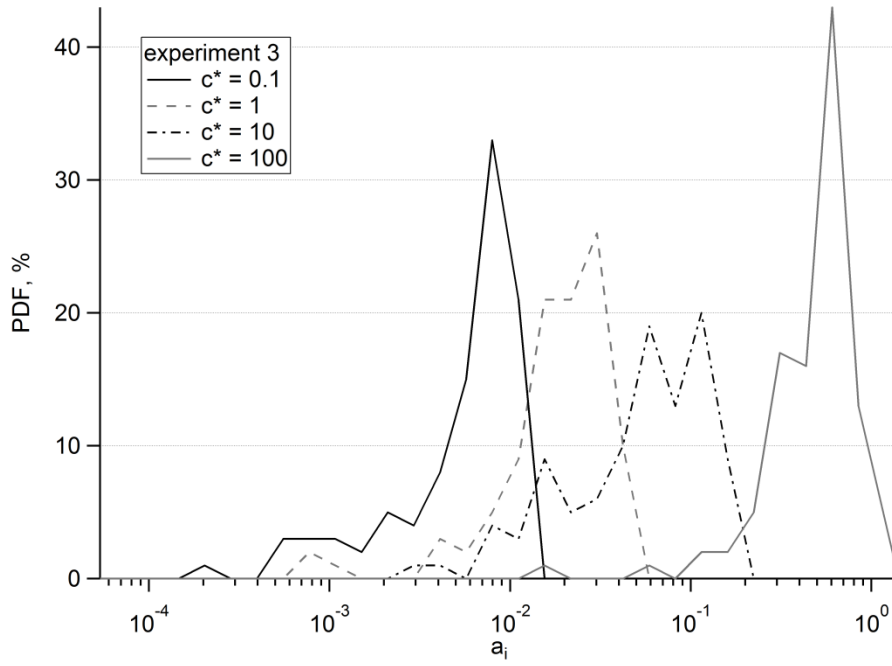
Figure 6. Probability density functions (PDF) of α_i's for volatility bins (C_i^* = 0.01, 0.1, 1, 10 and 100 μg m^{-3}) for one high *RH* (exp. 3, upper panel) experiment and one low *RH* (exp. 4, lower panel).
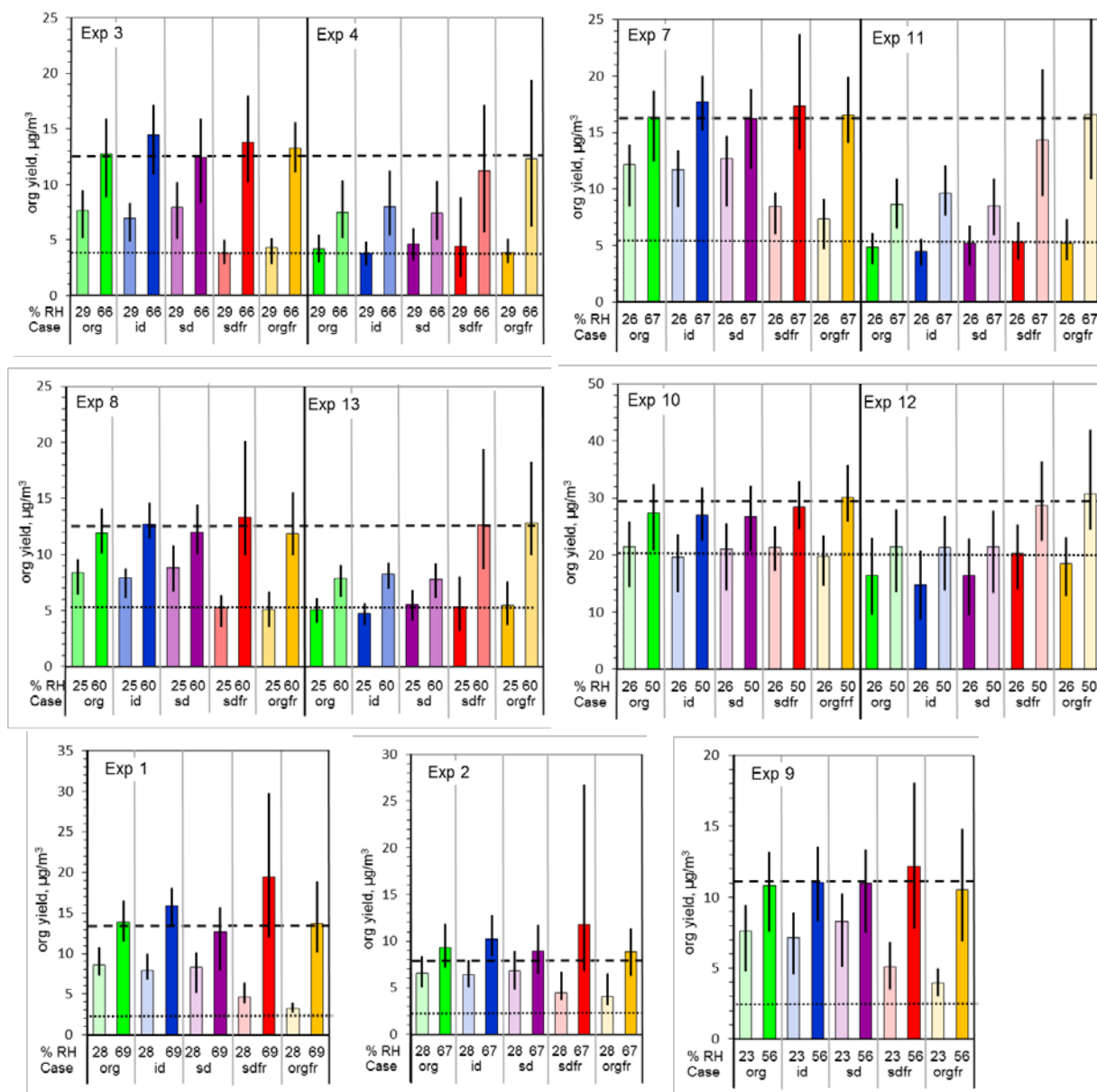
Figure 7. Calculated average organic yields for experiments at the measured RH (columns in full colors) and at the RH of the corresponding experiments (light colors, see Table 2 for reference) based on ten randomly chosen volatility distributions for the cases org, id, sd, sdfr, and orgfr (identified by different colors). The vertical black lines on the columns indicate the range of values obtained for the calculations with the individual volatility distributions. The horizontal dotted line marks the measured value for the experiment performed at low RH, the dashed line the value for the experiment performed at high RH.
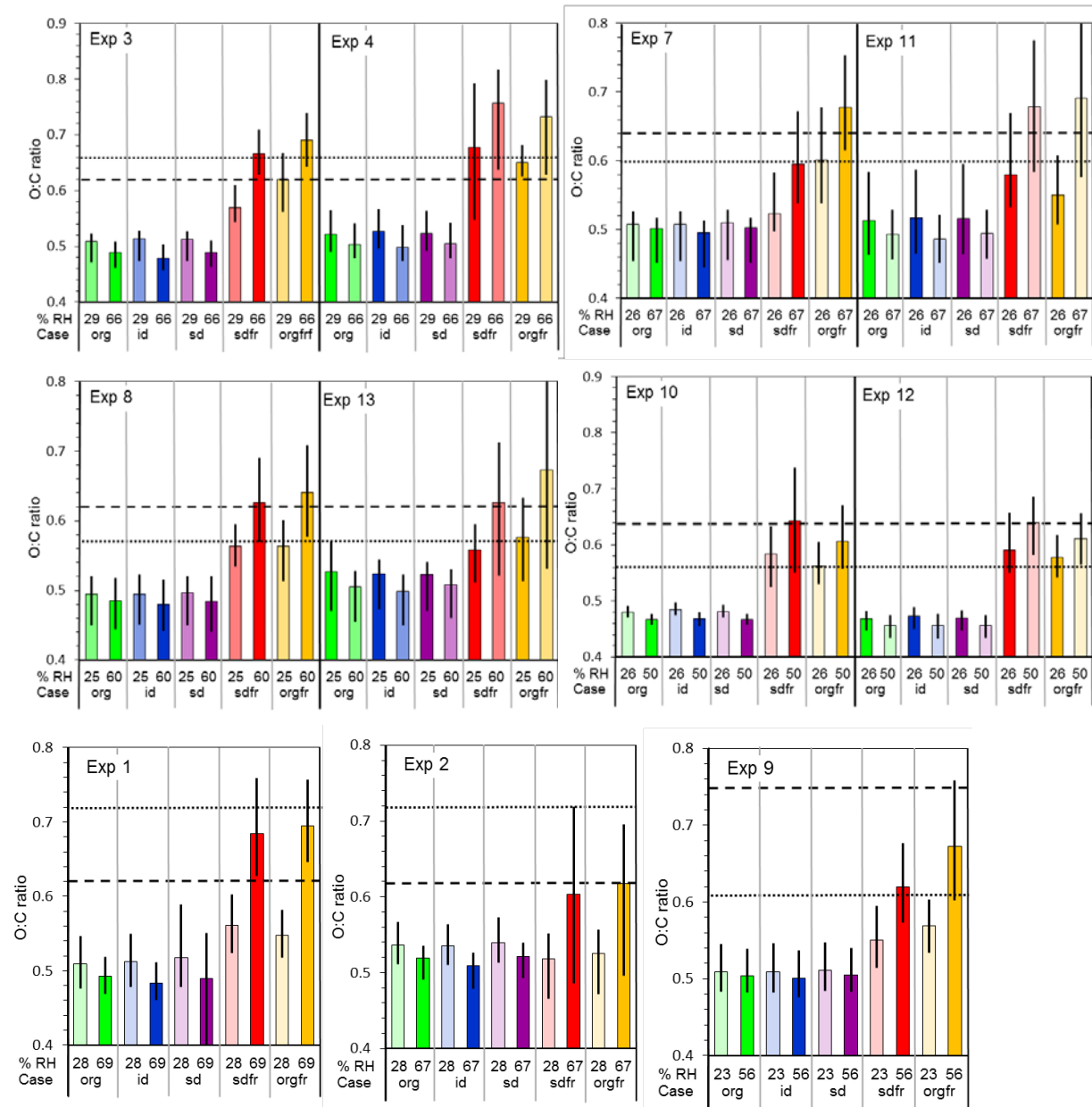
Figure 8. Calculated average O:C ratios for experiments at the measured RH (columns in full colors) and at the RH of the corresponding experiments (light colors, see Table 2 for reference) based on ten randomly chosen volatility distributions for the cases org, id, sd, sdfr, and orgfr (identified by different colors). The vertical black lines on the columns indicate the range of values obtained for the calculations with the individual volatility distributions. The horizontal dotted line marks the measured value for the experiment performed at low RH, the dashed line the value for the experiment performed at high RH.

45
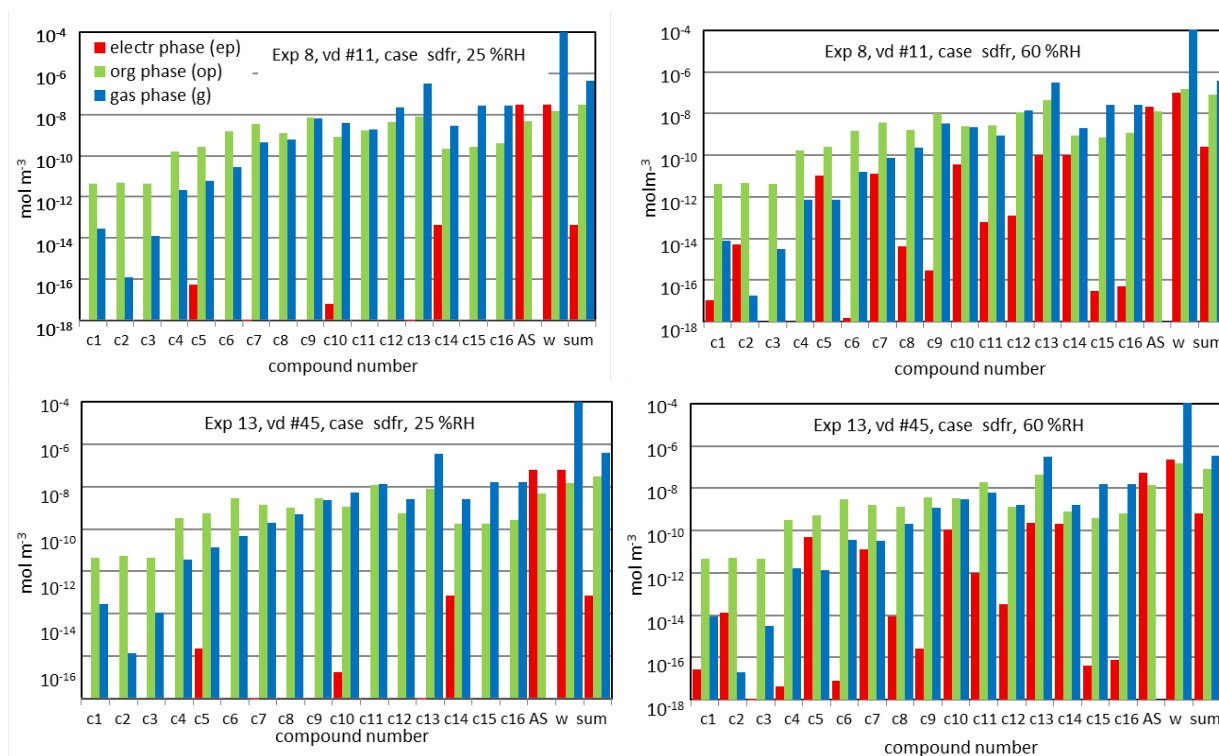
Figure 9. Equilibrium phase partitioning (mol m^{-3}) for case sdfr between gas phase, electrolyte phase, and organic phase at low RH (25 %) and at high RH (60 %) for experiment 8, volatility distribution #11 (upper panels) and experiment 13, volatility distribution #45 (lower panels). Compound numbers are c1: diaterpenylic acid acetate; c2: 3-MBTCA, c3: ValT4N9, c4: ValT4N10, c5: 3-hydroxyglutaric acid, c6: ValT4N3, c7: 3-oxoadipic acid; c8: pinic acid, c9: hopinonic acid, c10: glutaric acid: c11 norpinic acid, c12: 2-hydroxyterpenylic acid, c13: 5-COOH-3-OH-pentanal, c14: succinic acid, c15: 10-oxopinonic acid, c16: 4-oxopinonic acid, ammonium sulfate (AS), water (w), and the sum of compounds c1-c16.

50
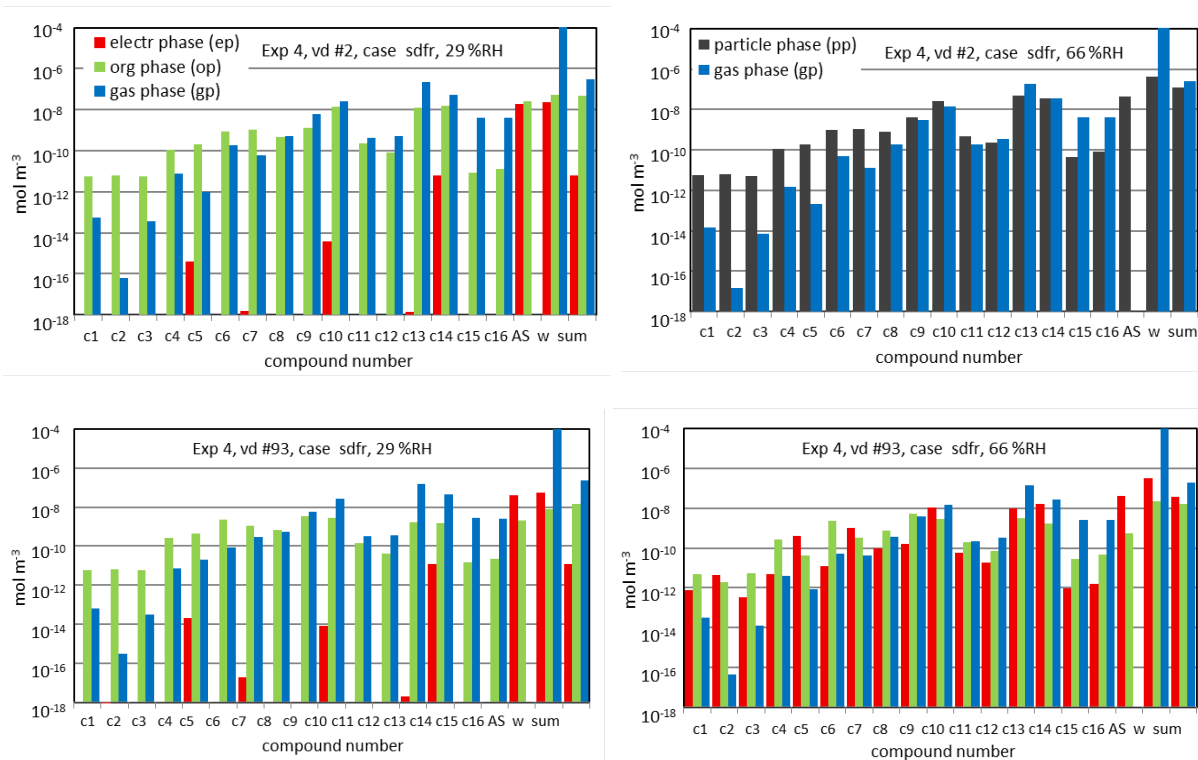
55

Figure 10. Equilibrium phase partitioning (mol m^{-3}) for case sdfr between gas phase, particle phase, electrolyte phase, and organic-rich phase at low (29 %) and high (66 %) RH for experiment 4, volatility distribution #2 (upper panels), and volatility distribution #93 (lower panels). Compound numbers are c1: diaterpenylic acid acetate; c2: 3-MBTCA, c3: ValT4N9, c4: ValT4N10, c5: 3-hydroxyglutaric acid, c6: ValT4N3, c7: 3-oxoadipic acid; c8: pinic acid, c9: hopinonic acid, c10: glutaric acid: c11 norpinic acid, c12: 2-hydroxyterpenylic acid, c13: 5-COOH-3-OH-pentanal, c14: succinic acid, c15: 10-oxopinonic acid, c16: 4-oxopinonic acid, ammonium sulfate (AS), water (w), and the sum of compounds c1-c16.

60

References

65 Aiken, A. C., DeCarlo, P. F., and Jimenez, J. L.: Elemental analysis of organic species with electron ionization high-resolution mass spectrometry, Anal. Chem., 79, 8350 - 8358, 2007.

Aiken, A. C., DeCarlo, P. F., Kroll, J. H., Worsnop, D. R., Huffman, J. A., Docherty, K. S., Ulbrich, I. M., Mohr, C., Kimmel, J. R., Sueper, D., Sun, Y., Zhang, Q., Trimborn, A., Northway, M., Ziemann, P. J., Canagaratna, M. R., Onasch, T. B., Alfarra, M. R., Prevot, A.

70 S. H., Dommen, J., Duplissy, J., Metzger, A., Baltensperger, U., and Jimenez, J. L.: O/C and OM/OC ratios of primary, secondary, and ambient organic aerosols with high-resolution time-of-flight aerosol mass spectrometry, Environ. Sci. Technol., 42, 4478-4485, 2008.

Atkinson, R.: Atmospheric chemistry of VOCs and NO_x, Atmos. Environ., 34, 2063-2101, 2000.

75 Atkinson, R., and Arey, J.: Gas-phase tropospheric chemistry of biogenic volatile organic compounds: a review, Atmos. Environ., 37, Supplement 2, 197-219, dx.doi.org/10.1016/S1352-2310(03)00391-1, 2003.

Barmet, P., Dommen, J., DeCarlo, P. F., Tritscher, T., Praplan, A. P., Platt, S. M., Prevot, A. S. H., Donahue, N. M., and Baltensperger, U.: OH clock determination by proton transfer

80 reaction mass spectrometry at an environmental chamber, Atmos. Meas. Tech., 5, 647-656, doi: 10.5194/amt-5-647-2012, 2012.

Bilde, M., Barsanti, K., Booth, M., Cappa, C. D., Donahue, N. M., Emanuelsson, E. U., McFiggans, G., Krieger, U. K., Marcolli, C., Topping, D., Ziemann, P., Barley, M., Clegg, S., Dennis-Smither, B., Hallquist, M., Hallquist, Å. M., Khlystov, A., Kulmala, M., Mogensen,

85 D., Percival, C. J., Pope, F., Reid, J. P., Ribeiro da Silva, M. A. V., Rosenoern, T., Salo, K., Soonsin, V. P., Yli-Juuti, T., Prisle, N. L., Pagels, J., Rarey, J., Zardini, A. A., and Riipinen, I.: Saturation vapor pressures and transition enthalpies of low-volatility organic molecules of atmospheric relevance: From dicarboxylic acids to complex mixtures, Chem. Rev. (Washington, DC, U. S.), 115, 4115-4156, doi: 10.1021/cr5005502, 2015.

90 Bonn, B., Schuster, G., and Moortgat, G. K.: Influence of water vapor on the process of new particle formation during monoterpene ozonolysis, J. Phys. Chem. A, 106, 2869-2881, 2002.

Bozzetti, C., Sosedova, Y., Xiao, M., Daellenbach, K. R., Ulevicius, V., Dudoitis, V., Mordas, G., Byčenkienė, S., Plauškaitė, K., Vlachou, A., Golly, B., Chazeau, B., Besombes, J. L., Baltensperger, U., Jaffrezo, J. L., Slowik, J. G., El Haddad, I., and Prévôt, A. S. H.:

95 Argon offline-AMS source apportionment of organic aerosol over yearly cycles for an urban, rural, and marine site in northern Europe, Atmos. Chem. Phys., 17, 117-141, 10.5194/acp-17-117-2017, 2017.

Canagaratna, M. R., Jayne, J. T., Jimenez, J. L., Allan, J. D., Alfarra, M. R., Zhang, Q., Onasch, T. B., Drewnick, F., Coe, H., Middlebrook, A., Delia, A., Williams, L. R., Trimborn,

100 A. M., Northway, M. J., DeCarlo, P. F., Kolb, C. E., Davidovits, P., and Worsnop, D. R.: Chemical and microphysical characterization of ambient aerosols with the Aerodyne aerosol mass spectrometer, Mass Spectrom. Rev., 26, 185-222, 2007.

Canagaratna, M. R., Jimenez, J. L., Kroll, J. H., Chen, Q., Kessler, S. H., Massoli, P., Hildebrandt Ruiz, L., Fortner, E., Williams, L. R., Wilson, K. R., Surratt, J. D., Donahue, N.

105 M., Jayne, J. T., and Worsnop, D. R.: Elemental ratio measurements of organic compounds using aerosol mass spectrometry: characterization, improved calibration, and implications, Atmos. Chem. Phys., 15, 253-272, doi: 10.5194/acp-15-253-2015, 2015.

Chang, R. Y. W., Slowik, J. G., Shantz, N. C., Vlasenko, A., Liggio, J., Sjostedt, S. J., Leaitch, W. R., and Abbatt, J. P. D.: The hygroscopicity parameter (κ) of ambient organic

110   aerosol at a field site subject to biogenic and anthropogenic influences: relationship to degree of aerosol oxidation, Atmos. Chem. Phys., 10, 5047-5064, doi: 10.5194/acp-10-5047-2010, 2010.

Chhabra, P. S., Lambe, A. T., Canagaratna, M. R., Stark, H., Jayne, J. T., Onasch, T. B., Davidovits, P., Kimmel, J. R., and Worsnop, D. R.: Application of high-resolution time-of-
115   flight chemical ionization mass spectrometry measurements to estimate volatility distributions of α-pinene and naphthalene oxidation products, Atmos. Meas. Tech., 8, 1-18, doi: 10.5194/amt-8-1-2015, 2015.

Ciobanu, V. G., Marcolli, C., Krieger, U. K., Zuend, A., and Peter, T.: Efflorescence of ammonium sulfate and coated ammonium sulfate particles: Evidence for surface nucleation,
120   The Journal of Physical Chemistry A, 114, 9486-9495, doi: 10.1021/jp103541w, 2010.

Clegg, S., Kleeman, M., Griffin, R., and Seinfeld, J.: Effects of uncertainties in the thermodynamic properties of aerosol components in an air quality model–Part 2: Predictions of the vapour pressures of organic compounds, Atmos. Chem. Phys., 8, 1087-1103, 2008a.

Clegg, S., Kleeman, M., Griffin, R., and Seinfeld, J.: Effects of uncertainties in the
125   thermodynamic properties of aerosol components in an air quality model–Part 1: Treatment of inorganic electrolytes and organic compounds in the condensed phase, Atmos. Chem. Phys., 8, 1057-1085, 2008b.

Cocker, D. R. I., Clegg, S. L., Flagan, R. C., and Seinfeld, J. H.: The effect of water on gas–particle partitioning of secondary organic aerosol. Part I: α-pinene/ozone system, Atmos.
130   Environ., 35, 6049-6072, 2001.

Compernolle, S., Ceulemans, K., and Müller, J. F.: EVAPORATION: a new vapour pressure estimation methodfor organic molecules including non-additivity and intramolecular interactions, Atmos. Chem. Phys., 11, 9431-9450, 10.5194/acp-11-9431-2011, 2011.

DeCarlo, P. F., Kimmel, J. R., Trimborn, A., Northway, M. J., Jayne, J. T., Aiken, A. C.,
135   Gonin, M., Fuhrer, K., Horvath, T., Docherty, K. S., Worsnop, D. R., and Jimenez, J. L.: Field-deployable, high-resolution, time-of-flight aerosol mass spectrometer, Anal. Chem., 78, 8281-8289, 2006.

Donahue, N. M., Robinson, A. L., Stanier, C. O., and Pandis, S. N.: Coupled partitioning, dilution, and chemical aging of semivolatile organics, Environ. Sci. Technol., 40, 2635-2643,
140   2006.

Donahue, N. M., Epstein, S. A., Pandis, S. N., and Robinson, A. L.: A two-dimensional volatility basis set: 1. organic-aerosol mixing thermodynamics, Atmos. Chem. Phys., 11, 3303-3318, 2011.

Donahue, N. M., Henry, K. M., Mentel, T. F., Kiendler-Scharr, A., Spindler, C., Bohn, B.,
145   Brauers, T., Dorn, H. P., Fuchs, H., Tillmann, R., Wahner, A., Saathoff, H., Naumann, K.-H., Möhler, O., Leisner, T., Müller, L., Reinnig, M.-C., Hoffmann, T., Salo, K., Hallquist, M., Frosch, M., Bilde, M., Tritscher, T., Barmet, P., Praplan, A. P., DeCarlo, P. F., Dommen, J., Prévôt, A. S. H., and Baltensperger, U.: Aging of biogenic secondary organic aerosol via gas-phase OH radical reactions, Proc. Natl. Acad. Sci. U. S. A., 109, 13503-13508, doi:
150   10.1073/pnas.1115186109, 2012a.

Donahue, N. M., Kroll, J. H., Pandis, S. N., and Robinson, A. L.: A two-dimensional volatility basis set – Part 2: Diagnostics of organic-aerosol evolution, Atmos. Chem. Phys., 12, 615-634, doi: 10.5194/acp-12-615-2012, 2012b.

Eddingsaas, N. C., Loza, C. L., Yee, L. D., Chan, M., Schilling, K. A., Chhabra, P. S.,
155   Seinfeld, J. H., and Wennberg, P. O.: α-pinene photooxidation under controlled chemical

conditions - Part 2: SOA yield and composition in low- and high-NO_x environments, Atmos. Chem. Phys., 12, 7413-7427, 2012.

El Haddad, I., D'Anna, B., Temime-Roussel, B., Nicolas, M., Boreave, A., Favez, O., Voisin, D., Sciare, J., George, C., Jaffrezo, J. L., Wortham, H., and Marchand, N.: Towards a better understanding of the origins, chemical composition and aging of oxygenated organic aerosols: case study of a Mediterranean industrialized environment, Marseille, Atmos. Chem. Phys., 13, 7875-7894, doi: 10.5194/acp-13-7875-2013, 2013.

Farmer, D., Matsunaga, A., Docherty, K., Surratt, J., Seinfeld, J., Ziemann, P., and Jimenez, J.: Response of an aerosol mass spectrometer to organonitrates and organosulfates and implications for atmospheric chemistry, Proc. Natl. Acad. Sci. U. S. A., 107, 6670-6675, 2010.

Hildebrandt, L., Henry, K. M., Kroll, J. H., Worsnop, D. R., Pandis, S. N., and Donahue, N. M.: Evaluating the mixing of organic aerosol components using high-resolution aerosol mass spectrometry, Environ. Sci. Technol., 45, 6329-6335, 2011.

Hoyle, C. R., Boy, M., Donahue, N. M., Fry, J. L., Glasius, M., Guenther, A., Hallar, A. G., Huff Hartz, K., Petters, M. D., Petäjä, T., Rosenoern, T., and Sullivan, A. P.: A review of the anthropogenic influence on biogenic secondary organic aerosol, Atmos. Chem. Phys., 11, 321-343, 2011.

Huisman, A. J., Krieger, U. K., Zuend, A., Marcolli, C., and Peter, T.: Vapor pressures of substituted polycarboxylic acids are much lower than previously reported, Atmos. Chem. Phys., 13, 6647-6662, doi: 10.5194/acp-13-6647-2013, 2013.

Iinuma, Y., Müller, C., Böge, O., Gnauk, T., and Herrmann, H.: The formation of organic sulfate esters in the limonene ozonolysis secondary organic aerosol (SOA) under acidic conditions, Atmos. Environ., 41, 5571-5583, 2007.

Jang, M., Czoschke, N. M., Lee, S., and Kamens, R. M.: Heterogeneous atmospheric aerosol production by acid-catalyzed particle-phase reactions, Science, 298, 814-817, 2002.

Jaoui, M., and Kamens, R. M.: Mass balance of gaseous and particulate products analysis from α-pinene/NOx/air in the presence of natural sunlight, Journal of Geophysical Research, 106, 12541–12558, doi: 10.1029/2001JD900005, 2001.

Jimenez, J. L., Canagaratna, M. R., Donahue, N. M., Prevot, A. S. H., Zhang, Q., Kroll, J. H., DeCarlo, P. F., Allan, J. D., Coe, H., Ng, N. L., Aiken, A. C., Docherty, K. S., Ulbrich, I. M., Grieshop, A. P., Robinson, A. L., Duplissy, J., Smith, J. D., Wilson, K. R., Lanz, V. A., Hueglin, C., Sun, Y. L., Tian, J., Laaksonen, A., Raatikainen, T., Rautiainen, J., Vaattovaara, P., Ehn, M., Kulmala, M., Tomlinson, J. M., Collins, D. R., Cubison, M. J., E, Dunlea, J., Huffman, J. A., Onasch, T. B., Alfarra, M. R., Williams, P. I., Bower, K., Kondo, Y., Schneider, J., Drewnick, F., Borrmann, S., Weimer, S., Demerjian, K., Salcedo, D., Cottrell, L., Griffin, R., Takami, A., Miyoshi, T., Hatakeyama, S., Shimono, A., Sun, J. Y., Zhang, Y. M., Dzepina, K., Kimmel, J. R., Sueper, D., Jayne, J. T., Herndon, S. C., Trimborn, A. M., Williams, L. R., Wood, E. C., Middlebrook, A. M., Kolb, C. E., Baltensperger, U., and Worsnop, D. R.: Evolution of organic aerosols in the atmosphere, Science, 326, 1525-1529, doi: 10.1126/science.1180353, 2009.

Jonsson, Å. M., Hallquist, M., and Ljungström, E.: Impact of humidity on the ozone initiated oxidation of limonene, Δ3-carene, and α-pinene, Environ. Sci. Technol., 40, 188-194, doi: 10.1021/es051163w, 2006.

200   Kleindienst, T. E., Edney, E. O., Lewandowski, M., Offenberg, J. H., and Jaoui, M.: Secondary organic carbon and aerosol yields from the irradiations of isoprene and α-pinene in the presence of NO_x and SO_2, Environ. Sci. Technol., 40, 3807-3812, 2006.

Kleindienst, T. E., Jaoui, M., Lewandowski, M., Offenberg, J. H., Lewis, C. W., Bhave, P. V., and Edney, E. O.: Estimates of the contributions of biogenic and anthropogenic hydrocarbons
205   to secondary organic aerosol at a southeastern US location, Atmos. Environ., 41, 8288-8300, doi:10.1016/j.atmosenv.2007.06.045, 2007.

Koop, T., Bookhold, J., Shiraiwa, M., and Pöschl, U.: Glass transition and phase state of organic compounds: dependency on molecular properties and implications for secondary organic aerosols in the atmosphere, Phys. Chem. Chem. Phys., 13, 19238-19255, 2011.

210   Krapf, M., El Haddad, I., Bruns, Emily A., Molteni, U., Daellenbach, Kaspar R., Prévôt, André S. H., Baltensperger, U., and Dommen, J.: Labile peroxides in secondary organic aerosol, Chem, 1, 603-616, 10.1016/j.chempr.2016.09.007, 2016.

Krechmer, J. E., Pagonis, D., Ziemann, P. J., and Jimenez, J. L.: Quantification of gas-wall partitioning in teflon environmental chambers using rapid bursts of low-volatility oxidized
215   species generated in situ, Environ. Sci. Technol., 50, 5757-5765, 10.1021/acs.est.6b00606, 2016.

Kreidenweis, S. M., Koehler, K., DeMott, P. J., Prenni, A. J., Carrico, C., and Ervens, B.: Water activity and activation diameters from hygroscopicity data – Part I: Theory and application to inorganic salts, Atmos. Chem. Phys., 5, 1357–1370, 2005.

220   Kroll, J. H., and Seinfeld, J. H.: Chemistry of secondary organic aerosol: Formation and evolution of low-volatility organics in the atmosphere, Atmos. Environ., 42, 3593-3624, 2008.

Li, Y., Pöschl, U., and Shiraiwa, M.: Molecular corridors and parameterizations of volatility in the chemical evolution of organic aerosols, Atmos. Chem. Phys., 16, 3327-3344, 10.5194/acp-16-3327-2016, 2016.

225   Loza, C. L., Chan, A. W. H., Galloway, M. M., Keutsch, F. N., Flagan, R. C., and Seinfeld, J. H.: Characterization of vapor wall loss in laboratory chambers, Environ. Sci. Technol., 44, 5074-5078, 10.1021/es100727v, 2010.

Marcolli, C., Luo, B. P., Peter, T., and Wienhold, F. G.: Internal mixing of the organic aerosol by gas phase diffusion of semivolatile organic compounds, Atmos. Chem. Phys., 2593-2599,
230   2004.

Marcolli, C., and Krieger, U. K.: Phase changes during hygroscopic cycles of mixed organic/inorganic model systems of tropospheric aerosols, The Journal of Physical Chemistry A, 110, 1881-1893, doi: 10.1021/jp0556759, 2006.

Martin, S. T.: Phase transitions of aqueous atmospheric particles, Chem. Rev. (Washington,
235   DC, U. S.), 100, 3403-3454, 2000.

Massoli, P., Lambe, A. T., Ahern, A. T., Williams, L. R., Ehn, M., Mikkilä, J., Canagaratna, M. R., Brune, W. H., Onasch, T. B., Jayne, J. T., Petäjä, T., Kulmala, M., Laaksonen, A., Kolb, C. E., Davidovits, P., and Worsnop, D. R.: Relationship between aerosol oxidation level and hygroscopic properties of laboratory generated secondary organic aerosol (SOA)
240   particles, Geophys. Res. Lett., 37, L24801, doi: 10.1029/2010GL045258, 2010.

Mutzel, A., Poulain, L., Berndt, T., Iinuma, Y., Rodigast, M., Böge, O., Richters, S., Spindler, G., Sipilä, M., Jokinen, T., Kulmala, M., and Herrmann, H.: Highly oxidized multifunctional organic compounds observed in tropospheric particles: a field and laboratory study, Environ. Sci. Technol., 49, 7754-7761, 10.1021/acs.est.5b00885, 2015.

245 Nah, T., McVay, R. C., Zhang, X., Boyd, C. M., Seinfeld, J. H., and Ng, N. L.: Influence of seed aerosol surface area and oxidation rate on vapor wall deposition and SOA mass yields: a case study with α-pinene ozonolysis, Atmos. Chem. Phys., 16, 9361-9379, 10.5194/acp-16-9361-2016, 2016.

Ng, N. L., Chhabra, P. S., Chan, A. W. H., Surratt, J. D., Kroll, J. H., Kwan, A. J., McCabe, 250 D. C., Wennberg, P. O., Sorooshian, A., Murphy, S. M., Dalleska, N. F., Flagan, R. C., and Seinfeld, J. H.: Effect of NO_x level on secondary organic aerosol (SOA) formation from the photooxidation of terpenes, Atmos. Chem. Phys., 7, 5159-5174, 2007.

Ng, N. L., Canagaratna, M. R., Jimenez, J. L., Chhabra, P. S., Seinfeld, J. H., and Worsnop, D. R.: Changes in organic aerosol composition with aging inferred from aerosol mass spectra, 255 Atmos. Chem. Phys., 11, 6465-6474, doi: 10.5194/acp-11-6465-2011, 2011a.

Nguyen, T. B., Tyndall, G. S., Crounse, J. D., Teng, A. P., Bates, K. H., Schwantes, R. H., Coggon, M. M., Zhang, L., Feiner, P., and Milller, D. O.: Atmospheric fates of Criegee intermediates in the ozonolysis of isoprene, Phys. Chem. Chem. Phys., 18, 10241-10254, 2016.

260 Odum, J. R., Hoffmann, T., Bowman, F., Collins, D., Flagan, R. C., and Seinfeld, J. H.: Gas/particle partitioning and secondary organic aerosol yields, Environ. Sci. Technol., 30, 2580-2585, doi: 10.1021/es950943+, 1996.

Pankow, J. F.: An absorption model of the gas/aerosol partitioning involved in the formation of secondary organic aerosol, Atmos. Environ., 28, 189-193, 1994.

265 Pankow, J. F.: Organic particulate material levels in the atmosphere: Conditions favoring sensitivity to varying relative humidity and temperature, Proc. Natl. Acad. Sci. U. S. A., 107, 6682-6686, doi: 10.1073/pnas.1001043107, 2010.

Paulsen, D., Dommen, J., Kalberer, M., Prévôt, A. S. H., Richter, R., Sax, M., Steinbacher, M., Weingartner, E., and Baltensperger, U.: Secondary organic aerosol formation by 270 irradiation of 1,3,5-trimethylbenzene-NO_x-H_2O in a new reaction chamber for atmospheric chemistry and physics, Environ. Sci. Technol., 39, 2668-2678, 2005.

Pfaffenberger, L., Barmet, P., Slowik, J. G., Praplan, A. P., Dommen, J., Prévôt, A. S. H., and Baltensperger, U.: The link between organic aerosol mass loading and degree of oxygenation: An α-pinene photooxidation study, Atmos. Chem. Phys., 13, 6493-6506, doi: 10.5194/acp-13-275 6493-2013, 2013.

Pieber, S. M., El Haddad, I., Slowik, J. G., Canagaratna, M. R., Jayne, J. T., Platt, S. M., Bozzetti, C., Daellenbach, K. R., Fröhlich, R., Vlachou, A., Klein, F., Dommen, J., Miljevic, B., Jiménez, J. L., Worsnop, D. R., Baltensperger, U., and Prévôt, A. S. H.: Inorganic salt interference on CO2+ in Aerodyne AMS and ACSM organic aerosol composition studies, 280 Environ. Sci. Technol., 50, 10494-10503, 10.1021/acs.est.6b01035, 2016.

Platt, S. M., El Haddad, I., Zardini, A. A., Clairotte, M., Astorga, C., Wolf, R., Slowik, J. G., Temime-Roussel, B., Marchand, N., Ježek, I., Drinovec, L., Močnik, G., Möhler, O., Richter, R., Barmet, P., Bianchi, F., Baltensperger, U., and Prévôt, A. S. H.: Secondary organic aerosol formation from gasoline vehicle emissions in a new mobile environmental reaction 285 chamber, Atmos. Chem. Phys., 13, 9141-9158, doi: 10.5194/acp-13-9141-2013, 2013.

Platt, S. M., Haddad, I. E., Pieber, S. M., Huang, R. J., Zardini, A. A., Clairotte, M., Suarez-Bertoa, R., Barmet, P., Pfaffenberger, L., Wolf, R., Slowik, J. G., Fuller, S. J., Kalberer, M., Chirico, R., Dommen, J., Astorga, C., Zimmermann, R., Marchand, N., Hellebust, S., Temime-Roussel, B., Baltensperger, U., and Prévôt, A. S. H.: Two-stroke scooters are a

290 dominant source of air pollution in many cities, Nature Communications, 5, 3749, 10.1038/ncomms4749, 2014.

Presto, A. A., Huff Hartz, K. E., and Donahue, N. M.: Secondary organic aerosol production from terpene ozonolysis. 2. Effect of NO_x concentration, Environ. Sci. Technol., 39, 7046-7054, doi: 10.1021/es050400s, 2005.

295 Prisle, N. L., Engelhart, G. J., Bilde, M., and Donahue, N. M.: Humidity influence on gas-particle phase partitioning of α-pinene + O_3 secondary organic aerosol, Geophys. Res. Lett., 37, L01802, doi: 10.1029/2009GL041402, 2010.

Robinson, E. S., Saleh, R., and Donahue, N. M.: Organic aerosol mixing observed by single-particle mass spectrometry, J. Phys. Chem., 13935–13945, doi: 10.1021/jp405789t, 2013.

300 Saleh, R., Donahue, N. M., and Robinson, A. L.: Time scales for gas-particle partitioning equilibration of secondary organic aerosol formed from alpha-pinene ozonolysis, Environ. Sci. Technol., 47, 5588-5594, doi: 10.1021/es400078d, 2013.

Shiraiwa, M., Yee, L. D., Schilling, K. A., Loza, C. L., Craven, J. S., Zuend, A., Ziemann, P. J., and Seinfeld, J. H.: Size distribution dynamics reveal particle-phase chemistry in organic
305 aerosol formation, Proc. Natl. Acad. Sci. U. S. A., 110, 11746-11750, doi: 10.1073/pnas.1307501110, 2013.

Song, M., Marcolli, C., Krieger, U. K., Zuend, A., and Peter, T.: Liquid-liquid phase separation and morphology of internally mixed dicarboxylic acids/ammonium sulfate/water particles, Atmos. Chem. Phys., 12, 2691-2712, doi: 10.5194/acp-12-2691-2012, 2012.

310 Stokes, R., and Robinson, R.: Interactions in aqueous nonelectrolyte solutions. I. Solute-solvent equilibria, J. Phys. Chem., 70, 2126-2131, 1966.

Taira, M., and Kanda, Y.: Continuous generation system for low-concentration gaseous nitrous acid, Anal. Chem., 62, 630-633, 1990.

Topping, D. O., McFiggans, G. B., and Coe, H.: A curved multi-component aerosol
315 hygroscopicity model framework: Part 1 – Inorganic compounds, Atmos. Chem. Phys., 5, 1205–1222, 2005.

Valorso, R., Aumont, B., Camredon, M., Raventos-Duran, T., Mouchel-Vallon, C., Ng, N. L., Seinfeld, J. H., Lee-Taylor, J., and Madronich, S.: Explicit modelling of SOA formation from α-pinene photooxidation: sensitivity to vapour pressure estimation, Atmos. Chem. Phys., 11,
320 6895-6910, doi: 10.5194/acp-11-6895-2011, 2011.

Virtanen, A., Joutsensaari, J., Koop, T., Kannosto, J., Yli-Pirila, P., Leskinen, J., Makela, J. M., Holopainen, J. K., Poschl, U., Kulmala, M., Worsnop, D. R., and Laaksonen, A.: An amorphous solid state of biogenic secondary organic aerosol particles, Nature, 467, 824-827, doi:10.1038/nature09455, 2010.

325 Williams, L. R., Gonzalez, L. A., Peck, J., Trimborn, D., McInnis, J., Farrar, M. R., Moore, K. D., Jayne, J. T., Robinson, W. A., Lewis, D. K., Onasch, T. B., Canagaratna, M. R., Trimborn, A., Timko, M. T., Magoon, G., Deng, R., Tang, D., Blanco, E., Prevot, A. S. H., Smith, K. A., and Worsnop, D. R.: Characterization of an aerodynamic lens for transmitting particles greater than 1 micrometer in diameter into the Aerodyne aerosol mass spectrometer,
330 Atmos. Meas. Tech., 6, 3271-3280, 2013.

Yatavelli, R. L. N., Stark, H., Thompson, S. L., Kimmel, J. R., Cubison, M. J., Day, D. A., Campuzano-Jost, P., Palm, B. B., Hodzic, A., Thornton, J. A., Jayne, J. T., Worsnop, D. R., and Jimenez, J. L.: Semicontinuous measurements of gas–particle partitioning of organic

acids in a ponderosa pine forest using a MOVI-HRToF-CIMS, Atmos. Chem. Phys., 14,
335   1527-1546, doi: 10.5194/acp-14-1527-2014, 2014.

You, Y., Renbaum-Wolff, L., and Bertram, A. K.: Liquid–liquid phase separation in particles
containing organics mixed with ammonium sulfate, ammonium bisulfate, ammonium nitrate
or sodium chloride, Atmos. Chem. Phys., 13, 11723-11734, doi: 10.5194/acp-13-11723-2013,
2013.

340   You, Y., Smith, M. L., Song, M., Martin, S. T., and Bertram, A. K.: Liquid–liquid phase
separation in atmospherically relevant particles consisting of organic species and inorganic
salts, Int. Rev. Phys. Chem., 33, 43-77, doi: 10.1080/0144235X.2014.890786, 2014.

Zhang, X., Cappa, C. D., Jathar, S. H., McVay, R. C., Ensberg, J. J., Kleeman, M. J., and
Seinfeld, J. H.: Influence of vapor wall loss in laboratory chambers on yields of secondary
345   organic aerosol, Proceedings of the National Academy of Sciences, 111, 5802-5807,
10.1073/pnas.1404727111, 2014.

Zhang, X., Schwantes, R. H., McVay, R. C., Lignell, H., Coggon, M. M., Flagan, R. C., and
Seinfeld, J. H.: Vapor wall deposition in Teflon chambers, Atmos. Chem. Phys., 15, 4197-
4214, 10.5194/acp-15-4197-2015, 2015.

350   Zuend, A., Marcolli, C., Luo, B. P., and Peter, T.: A thermodynamic model of mixed organic-
inorganic aerosols to predict activity coefficients, Atmos. Chem. Phys., 8, 4559-4593, doi:
10.5194/acp-8-4559-2008, 2008.

Zuend, A., Marcolli, C., Peter, T., and Seinfeld, J. H.: Computation of liquid-liquid equilibria
and phase stabilities: implications for RH-dependent gas/particle partitioning of organic-
355   inorganic aerosols, Atmos. Chem. Phys., 10, 7795-7820, doi: 10.5194/acp-10-7795-2010,
2010.

Zuend, A., Marcolli, C., Booth, A. M., Lienhard, D. M., Soonsin, V., Krieger, U. K., Topping,
D. O., McFiggans, G., Peter, T., and Seinfeld, J. H.: New and extended parameterization of
the thermodynamic model AIOMFAC: calculation of activity coefficients for organic-
360   inorganic mixtures containing carboxyl, hydroxyl, carbonyl, ether, ester, alkenyl, alkyl, and
aromatic functional groups, Atmos. Chem. Phys., 11, 9155-9206, doi: 10.5194/acp-11-9155-
2011, 2011.

Zuend, A., and Seinfeld, J. H.: Modeling the gas-particle partitioning of secondary organic
aerosol: the importance of liquid-liquid phase separation, Atmos. Chem. Phys., 12, 3857-
365   3882, doi: 10.5194/acp-12-3857-2012, 2012.

Zuend, A., and Seinfeld, J. H.: A practical method for the calculation of liquid–liquid
equilibria in multicomponent organic–water–electrolyte systems using physicochemical
constraints, Fluid Phase Equilib., 337, 201-213, doi: 10.1016/j.fluid.2012.09.034, 2013.

370